

# An Approach Toward the Numerical Evaluation of Multi-Loop Feynman Diagrams

GIAMPIERO PASSARINO\*

*Dipartimento di Fisica Teorica, Università di Torino, Italy*  
*INFN, Sezione di Torino, Italy*

A scheme for systematically achieving accurate numerical evaluation of multi-loop Feynman diagrams is developed. This shows the feasibility of a project aimed to produce a complete calculation for two-loop predictions in the Standard Model. As a first step an algorithm, proposed by F. V. Tkachov and based on the so-called generalized Bernstein functional relation, is applied to one-loop multi-leg diagrams with particular emphasis to the presence of infrared singularities, to the problem of tensorial reduction and to the classification of all singularities of a given diagram. Successively, the extension of the algorithm to two-loop diagrams is examined. The proposed solution consists in applying the functional relation to the one-loop sub-diagram which has the largest number of internal lines. In this way the integrand can be made smooth, a part from a factor which is a polynomial in  $x_s$ , the vector of Feynman parameters needed for the complementary sub-diagram with the smallest number of internal lines. Since the procedure does not introduce new singularities one can distort the  $x_s$ -integration hyper-contour into the complex hyper-plane, thus achieving numerical stability. The algorithm is then modified to deal with numerical evaluation around normal thresholds. Concise and practical formulas are assembled and presented, numerical results and comparisons with the available literature are shown and discussed for the so-called sunset topology.

PACS Classification: 11.10.-z; 11.15.Bt; 12.38.Bx; 02.90.+p

---

\*Work supported by the European Union under contract HPRN-CT-2000-00149.

# 1 Introduction

The evaluation of multi-loop Feynman diagrams has a long history dating back to the days of renormalization of QED (for an historical review see ref. [1]). In this respect there are theories more simple than others, noticeably QED and also to some extent QCD, where we have few masses and the analytical approach can be pushed very far. Typical examples are the calculations of  $g-2$  in QED, see for instance ref. [2], or recent four-loop calculations in QCD [4]. Conversely the full electroweak Lagrangian shows several masses, ranging over a wide interval of values, therefore making the analytical evaluation of Feynman diagrams a complicated task.

The modern era of loop-calculus begins with the work of 't Hooft and Veltman [5] for arbitrary one-loop diagrams. As a result, an arbitrary scalar triangle diagram is expressed as the combination of 12 di-logarithms (sometimes called Spence-functions) while 108 di-logarithms are needed for the general box diagram.

In recent years we have been witnessing a huge amount of work in the direction of analytical evaluation of multi-loop diagrams. To be more precise we should distinguish between reduction procedures to bring specific classes of physics problems to some specific classes of integrals and calculational procedures for those specific classes of integrals.

It would be impossible to quote the hundreds of papers that have been dealing with the subject and we are forced to make some selection. In the following we will briefly review the relevant literature, confining the search to those papers that are not directly connected to the present work. Other important references will appear in the body of the paper.

Following and improving the techniques of [5] dimensionally regulated pentagon integrals have been considered in [6]. At the same time the methodology for one-loop  $n$ -point gauge theory amplitudes has been further developed in [7] and in [8].

The algebraic reduction of one loop graphs, introduced in [9], has been reconsidered in [10]. More generally, the problem of reducing Feynman graph amplitudes to a minimal set of basic integrals has been discussed in [11].

An example of systematic approach to multi-loop calculations with the use of the program SCHOONSCHIP [12] is due to the Dubna group and a summary of the results can be found in ref. [13]. Meanwhile, algebraic programs like Mincer have been introduced [14].

An important breakthrough in this line of research is also represented by the algebraic approach, the so-called method of integration by parts. The simplest identity of this type was buried in a proof in [58]. A complete summary of everything relevant for 3-loop self-energies, as used in the next-to-next order (NNLO) calculations, is collected in [15]. The concept and calculability of massless three-loop self-energies was reported in [16]. Further details for three-loop self-energies can be found in [17]. Also important in this context are explicit solutions of the recurrence relations, see for instance ref. [18].

Another line of development is related to the evaluation of massive integrals, e.g. in the context of effective heavy-mass theory. The most recent reference is [19]. Finally a group of people were successfully using the so-called method of uniqueness with various improvements, see ref. [20] and also [21],[22] and [23].

Another significant development is represented by the method of differential equations, first discussed in [24] and fully developed in [25] (see also ref. [26]). Explicit solutions of the recurrence relations with respect to space-time dimension are shown in [27]. Generalized recurrence relations for two-loop propagator integrals with arbitrary masses are discussed in [28].

Furthermore, there is the subject of asymptotic expansions of Feynman diagrams. The first journal report of existence of simple formulas for OPE (those used in NNLO calculations) was in ref. [29], while a summary of the rules was presented in ref. [30]. The euclidean variant of the theory appeared in ref. [31] and [39]. The theory was reviewed – and the key trick to extend it to Minkowski space indicated – in ref. [32]. The final step was the extension of the theory to arbitrary diagrams in Minkowski space (including real phase-space diagrams), see for instance ref. [33]. Successive contributions can be found in ref. [34].

The techniques of Gegenbauer polynomials has proven to be useful for massless self-energies, mostly in two loops but with non-canonical powers of propagators, see ref. [37] and ref. [38].

Another meaningful technique, namely momentum expansion of multi-loop Feynman diagrams, was introduced in [41]. Furthermore, the connection between Feynman integrals having different values of the space-time dimension was shown in [42], and the conformal mapping and Pade approximants to the calculation of various two-loop Feynman diagrams in [43].

Another significant attempt towards the analytical evaluation of multi-loop diagrams is represented by the work of ref. [44].

As far as applications to the standard model are concerned, two-loop self-energies have been discussed in [40]. From the point of view of calculations with a direct relevance to standard model phenomenology we quote the next-to-leading two-loop electroweak top corrections of ref. [45], the fermionic two-loop contributions to muon decay and  $M_W - M_Z$  interdependence of ref. [46] and the complete two-loop QED contributions to the muon lifetime [47].

All these approaches, with very few exceptions, have a common motivation: to compute analytically as much as possible of multi-loop Feynman diagrams. Soon or later this approach will collapse and one can easily foresee that this failure will show up at the level of a complete two-loop calculation in the standard model which is required to produce quantities as  $\sin^2 \theta_{\text{eff}}^l$  with a theoretical precision of  $1 \times 10^{-6}$ . For this reason one is lead to consider an alternative approach to the whole problem, namely to abandon the analytical way in favor of a fully automatic, numerical evaluation of multi-loop diagrams. The Holy Graal (General Recursive Applicative and Algorithmic Language) requires fast and accurate procedures to deal with the singularities of an arbitrary diagram.

The outline of the paper will be as follows: in Section 2 we briefly review the Bernstein-Tkachov (BT) theorem and in Section 2.1 we consider its application to one-loop diagrams. In particular, the infrared divergent triangle graph is discussed in Section 2.1.1, while other one-loop functions are studied in Section 2.1.2 and 2.1.3. Reduction of tensor one-loop integrals is examined in Section 2.1.4. Singularities of one-loop diagrams and the connection between generalized Bernstein functional relation and Landau singularities is briefly addressed in Section 2.1.5. Multi-loop diagrams are introduced in Section 2.2 and the main result of this paper, the minimal BT approach, is presented in Section 3. In Section 3.1 and 3.1.3 we discuss the evaluation of the so-called sunset

two-loop diagram (or sunrise, depending on the mood of the author). Integration with complex Feynman parameters is introduced in Section 3.1.4 and a solution for numerical evaluation around and at the normal threshold is given in Section 3.1.5. Special cases of the sunset diagram are discussed in Section 3.1.6 where numerical results are shown and comparison are performed with those results that are available in the literature. Tensor integrals are introduced and discussed in Section 3.2. Technical details are presented in several appendices.

## 2 Bernstein-Tkachov theorem

For a fast and accurate numerical evaluation of multi-loop diagrams there is some interesting proposal in the literature that has not yet received the due attention.

The Bernstein-Tkachov theorem tells us that for any finite set of polynomials  $V_i(x)$ , where  $x = (x_1, \dots, x_N)$  is a vector of Feynman parameters, there exists an identity of the following form:

$$\mathcal{P}(x, \partial) \prod_i V_i^{\mu_i+1}(x) = B \prod_i V_i^{\mu_i}(x). \quad (1)$$

where  $\mathcal{P}$  is a polynomial of  $x$  and  $\partial_i = \partial/\partial x_i$ ;  $B$  and all coefficients of  $\mathcal{P}$  are polynomials of  $\mu_i$  and of the coefficients of  $V_i(x)$ . The proof of the theorem uses methods of abstract algebra and we refer to the paper by F. V. Tkachov [50] for details. Given any Feynman diagram the  $\mu_i$  in Eq.(1) will be of the form  $-n_i - \varepsilon/2$  where  $n_i$  are positive integers and  $n = 4 - \varepsilon$  with  $n$  being the space-time dimension. One can apply recursively Eq.(1) till the moment when all powers are of the form  $N_i - \varepsilon/2$  with  $N_i \geq 0$ . The Laurent expansion in  $\varepsilon$  yields the final form of the integrand. As pointed out in ref.[51], with  $N_i = 0$  the imaginary part of the integrand is discontinuous, with  $N_i = 1$  the integrand is continuous, with  $N_i = 2$  has continuous first derivative and so on. In the next section we will show the solution for arbitrary one-loop diagrams.

### 2.1 The one-loop case

For arbitrary one-loop diagrams we have a universal master formula, again due to F. V. Tkachov [50] (see also ref. [51] and ref. [52]). Any one-loop Feynman diagram  $G$ , irrespectively from the number of external legs, is expressible as

$$G = \int_S dx V^{-\mu}(x), \quad (2)$$

where the integration region is  $x_i \geq 0$ ,  $\sum_i x_i \leq 1$  and where  $V(x)$  is a quadratic form of  $x$ ,

$$V(x) = x^t H x + 2 K^t x + L. \quad (3)$$

The solution to the problem of determining the polynomial  $\mathcal{P}$  is as follows:

$$\mathcal{P} = 1 - \frac{(x + X) \partial_x}{2(\mu + 1)}, \quad X = K^t H^{-1}, \quad B = L - K^t H^{-1} K. \quad (4)$$

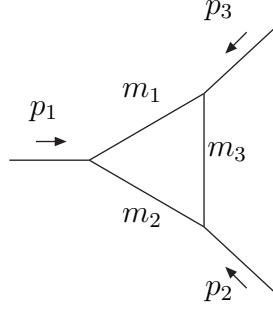


Figure 1: The three-point Green function. All external momenta are flowing inwards.

Let us consider an example, the scalar 3-point function  $C_0$  of Fig. 1. The corresponding expression is written in terms of a 2-dimensional integral. We start from

$$\begin{aligned} C_0 &\equiv C_0(p_1^2, p_2^2, (p_1 + p_2)^2; m_1, m_2, m_3) \\ &= \frac{\mu^\epsilon}{i\pi^2} \int d^n q \frac{1}{(q^2 + m_1^2) \left( (q + p_1)^2 + m_2^2 \right) \left( (q + p_1 + p_2)^2 + m_3^2 \right)}, \end{aligned} \quad (5)$$

where  $n = 4 - \epsilon$  is the space-time dimension and  $\mu$  is the arbitrary unit of mass. After introducing Feynman parameters, we obtain

$$C_0 = \int_0^1 dx \int_0^x dy V^{-1-\epsilon/2}(x, y), \quad V(x, y) = ax^2 + by^2 + cxy + dx + ey + f - i\delta \quad (6)$$

where  $\delta \rightarrow 0_+$  and where the coefficients of the quadratic form  $V$  are

$$\begin{aligned} a &= -p_2^2, & b &= -p_1^2, & c &= p_1^2 + p_2^2 - Q^2, & d &= p_2^2 + m_2^2 - m_3^2, \\ e &= -p_2^2 + Q^2 + m_1^2 - m_2^2, & f &= m_3^2. \end{aligned} \quad (7)$$

Therefore, the quadratic form in Feynman parameters is specified by

$$H = \frac{1}{2} \begin{pmatrix} 2a & c \\ c & 2b \end{pmatrix}, \quad K^t = \frac{1}{2} (d, e), \quad L = f - i\delta. \quad (8)$$

The main idea beyond the BT-theorem is that we can now integrate by parts and *raise powers* in the integrand. The first step will be as follows: define  $(X, Y) = (H^{-1})^t K$  and derive

$$\begin{aligned} C_0 &= \frac{1}{B} \left(1 - \frac{1}{\epsilon}\right) \int_0^1 dx \int_0^x dy V^{-\epsilon/2}(x, y) + \frac{1}{B\epsilon} \int_0^1 dx \left[ (1 + Y) V^{-\epsilon/2}(x, 1) \right. \\ &\quad \left. - Y V^{-\epsilon/2}(x, 0) + (1 + X) V^{-\epsilon/2}(1, x) - (x + X) V^{-\epsilon/2}(x, x) \right]. \end{aligned} \quad (9)$$

Although this formulas could be used directly as it stands, better numerical convergency is reached when we *raise* again the power of  $V$ . This requires applying again Eq.(4) to the first term in Eq.(9)

with  $\mu = -\epsilon$ . For the terms inside the second integral of Eq.(9) we have now several quadratic forms in one variable to which the algorithm has to be applied:

$$\begin{aligned}
1) \quad & V(x, 1) = ax^2 + (c + d)x + b + e + f - i\delta \\
2) \quad & V(x, 0) = ax^2 + dx + f - i\delta \\
3) \quad & V(1, x) = bx^2 + (c + e)x + a + d + f - i\delta \\
4) \quad & V(x, x) = (a + b + c)x^2 + (d + e)x + f - i\delta.
\end{aligned} \tag{10}$$

The corresponding coefficients are

$$\begin{aligned}
1) \quad & H = a, \quad K = \frac{1}{2}(c + d), \quad L = b + e + f - i\delta; \\
2) \quad & H = a, \quad K = \frac{1}{2}d, \quad L = f - i\delta; \\
3) \quad & H = b, \quad K = \frac{1}{2}(c + e), \quad L = a + d + f - i\delta; \\
4) \quad & H = a + b + c, \quad K = \frac{1}{2}(d + e), \quad L = f - i\delta.
\end{aligned} \tag{11}$$

The full result can be represented as the sum of a two-dimensional integral, a one-dimensional integral and a remainder,

$$C_0 = \Delta^{-1} \left[ \Delta^{-1} C_0^d + C_0^s + C_0^0 \right]. \tag{12}$$

Several combinations of the external parameters, not to be confused with Gram's determinants, enter into the final expression. They are

$$G_2 = 4ab - c^2, \quad G_{11} = a + b + c, \quad G_{12} = a, \quad G_{13} = b. \tag{13}$$

From them additional auxiliary quantities are constructed,

$$\begin{aligned}
\Delta &= fG_2 - (bd^2 - cde + ae^2), \\
\Delta_1 &= fG_{11} - \frac{(d + e)^2}{4}, \quad \Delta_2 = fG_{12} - \frac{d^2}{4}, \quad \Delta_3 = (a + d + f),
\end{aligned} \tag{14}$$

and also

$$\begin{aligned}
a_x &= 2db - ce, \quad a_y = 2ea - dc, \\
a_{1x} &= \frac{d + e}{2}, \quad a_{2x} = \frac{d}{2}, \quad a_{3x} = \frac{c + e}{2}.
\end{aligned} \tag{15}$$

The three contributions of Eq.(12) will then be written in terms of the auxiliary function  $V_L(x, y) = V(x, y) \ln V(x, y)$ . We obtain

$$C_0^d = 2G_2^2 \int_0^1 dx \int_0^x dy V_L(x, y), \tag{16}$$

$$C_0^s = \frac{1}{2} \int_0^1 dx \left\{ V_L(x, x)(a_x - a_y) \left[ G_2 \Delta^{-1} + \frac{3}{2} G_{11} \Delta_1^{-1} \right] + V_L(x, 0) a_y \left[ G_2 \Delta^{-1} + \frac{3}{2} G_{12} \Delta_2^{-1} \right] \right\}$$

$$- V_L(1, x) \left[ G_2 \left( \Delta^{-1} a_x + \frac{3}{2} G_{13} \Delta_3^{-1} + \frac{1}{2} G_2 \right) + \frac{3}{2} a_x G_{13} \Delta_3^{-1} \right], \quad (17)$$

$$\begin{aligned} C_0^0 = & -\frac{1}{4} G_2 \Delta_3^{-1} \left[ a_{3x} (b + c + e) + \frac{1}{2} G_{13} \left( \frac{4}{3} b + c + e \right) \right] \\ & + \frac{1}{12} G_2^2 \Delta^{-1} (3a + b + \frac{3}{2} c + 4d + 2e + 6f) + \frac{1}{4} a_x a_{1x} \Delta_1^{-1} (a + b + c + d + e) \\ & - \frac{1}{4} a_x a_{3x} \Delta_3^{-1} (b + c + e) + \frac{1}{6} a_x G_{11} \Delta_1^{-1} (a + b + c + \frac{3}{4} d + \frac{3}{4} e) \\ & - \frac{1}{8} a_x G_{13} \Delta_3^{-1} \left( \frac{4}{3} b + c + e \right) - \frac{1}{4} a_y a_{1x} \Delta_1^{-1} (a + b + c + d + e) \\ & + \frac{1}{4} a_y a_{2x} \Delta_2^{-1} (a + d) - \frac{1}{6} a_y G_{11} \Delta_1^{-1} (a + b + c + \frac{3}{4} d + \frac{3}{4} e) + \frac{1}{6} a_y G_{12} \Delta_2^{-1} (a + \frac{3}{4} d) \\ & + \frac{1}{4} V_L(0, 0) \left[ a_x a_{1x} \Delta_1^{-1} - a_y a_{1x} \Delta_1^{-1} + a_y a_{2x} \Delta_2^{-1} \right] \\ & - \frac{1}{4} V_L(1, 0) \left[ G_2 a_{3x} \Delta_3^{-1} + a_x a_{3x} \Delta_3^{-1} + 4 a_y a_{2x} \Delta_2^{-1} + a_y G_{12} \Delta_2^{-1} \right] \\ & + \frac{1}{4} V_L(1, 1) \left[ G_2 a_{3x} \Delta_3^{-1} + G_2 G_{13} \Delta_3^{-1} - a_x a_{1x} \Delta_1^{-1} + a_x a_{3x} \Delta_3^{-1} \right. \\ & \left. - a_x G_{11} \Delta_1^{-1} + a_x G_{13} \Delta_3^{-1} + a_y a_{1x} \Delta_1^{-1} + a_y G_{11} \Delta_1^{-1} \right]. \quad (18) \end{aligned}$$

It should be mentioned that in this approach the number of terms of the integrand really does not matter. The only relevant request to be made is that the algorithm is capable of producing a smooth integrand. Furthermore the algorithm should be flexible enough to deal with all singularities, including infrared ones.

### 2.1.1 Infrared divergent $C_0$ -function

As a first example that this method can handle infrared divergences (IR) in the context of dimensional regularization we consider the case of the IR-divergent  $C_0$ -function. From Eq.(4) one can prove that  $B = 0$  when

$$a = b = f = m^2, \quad c = e = s - 2m^2, \quad d = -2m^2, \quad (19)$$

i.e. for the case where an infrared divergency is developed. Here we introduced  $s = -(p_1 + p_2)^2$ . Since the zeros of  $B$  correspond to leading Landau singularities (see Section 2.1.5) we recover the connection between infrared singularities and the more general class of Landau ones: as shown in Eq.(19), an infrared singularity for  $C_0$  manifests itself independently of  $s$ . As a consequence we have that the quadratic form  $V$  satisfies the following equation:

$$\left[ 1 + P_x \frac{\partial}{\partial x} + P_y \frac{\partial}{\partial y} \right] V^{\mu+1}(x, y) = 0, \quad (20)$$

where the solution for the polynomial  $P$  is given by

$$P_{\{x;y\}} = \frac{\{1-x; -y\}}{2(\mu+1)}. \quad (21)$$

We use Eq.(20) to write

$$\int_0^1 dx \int_0^x dy V^{-1-\varepsilon/e}(x, y) = -\frac{1}{\varepsilon} \int_0^1 dx V^{-1-\varepsilon/e}(x, x). \quad (22)$$

Since the IR pole at  $n = 4$  will remain in the final answer we must keep trace of all  $n$ -dependent factors,

$$\begin{aligned} C_0(-m^2, -m^2, -s; m, 0, m) &= -\mu^\varepsilon \pi^{-\varepsilon/2} \Gamma\left(1 + \frac{\varepsilon}{2}\right) \frac{1}{\varepsilon} \int_0^1 dx V^{-1-\varepsilon/e}(x, x) \\ &= -\frac{1}{2} \mu^\varepsilon \frac{1}{\bar{\varepsilon}} \int_0^1 dx V^{-1-\varepsilon/e}(x, x), \end{aligned} \quad (23)$$

where we have introduced the usual ultraviolet and infrared regulators [53]

$$\frac{1}{\bar{\varepsilon}} = \frac{2}{\varepsilon} - \gamma - \ln \pi, \quad \frac{1}{\hat{\varepsilon}} = \frac{2}{\varepsilon'} + \gamma + \ln \pi, \quad (24)$$

and recall that these regulators satisfy the following relevant identity [53]:

$$\frac{1}{\bar{\varepsilon}} + \frac{1}{\hat{\varepsilon}} = 0. \quad (25)$$

Therefore, from Eq.(23) we recover the familiar result for the infrared  $C_0$ -function, see ref [53] and also ref. [5]. The power in  $V(x, x)$  can be *raised* once more with the help of the relation

$$\left[1 + \frac{1}{2(\mu+1)} \left(\frac{1}{2} - x\right) \partial_x\right] V^{1+\mu}(x, x) = -\frac{1}{4} (s - 4m^2) V^\mu(x, x). \quad (26)$$

Collecting the various terms we obtain the final expression for the  $C_0$ -function,

$$\begin{aligned} C_0^{\text{IR}} &= \frac{1}{s - 4m^2} \left\{ -\frac{1}{2} \frac{1}{\bar{\varepsilon}} \left[1 + \frac{1}{2} \int_0^1 dx \ln \frac{V(x, x)}{m^2}\right] - \frac{1}{2} \right. \\ &\quad \left. + \frac{1}{4} \ln \frac{m^2}{\mu^2} \left(1 + \frac{1}{2} \ln \frac{m^2}{\mu^2}\right) - \frac{1}{4} \int_0^1 dx \ln \frac{V(x, x)}{\mu^2} \left[3 + \frac{1}{2} \ln \frac{V(x, x)}{\mu^2}\right] \right\}. \end{aligned} \quad (27)$$

In conclusion the BT-algorithm automatically extracts the poles in  $n - 4$ , both ultraviolet and infrared.



### 2.1.2 Other one-loop functions

The procedure outlined above can be applied to any one-loop scalar function. Here we only show how it works for the massless pentagon (the massive case is as easy as the massless one). One can prove that

$$E_0 = \int_0^1 dx_1 \int_0^{1-x_1} dx_2 \int_0^{1-x_1-x_2} dx_3 \int_0^{1-x_1-x_2-x_3} dx_4 \left[ x^t H^{-1} x + 2 K^t x \right]^{-3-\varepsilon/2}, \quad (28)$$

where the  $4 \times 4$  matrix  $H$  is defined in terms of Mandelstam invariants,  $s_{ij} = -(p_i + p_j)^2$ , by the following form:

$$H = \frac{1}{2} \begin{pmatrix} 0 & -s_{51} & s_{12} - s_{34} & s_{45} \\ - & -2s_{51} & -s_{34} - s_{51} & s_{23} - s_{51} \\ - & - & -2s_{34} & -s_{34} \\ - & - & - & 0 \end{pmatrix}$$

and the vector  $K$  becomes

$$K_1 = 0, \quad K_2 = \frac{1}{2} s_{51}, \quad K_3 = \frac{1}{2} s_{34}, \quad K_4 = 0, \quad (29)$$

Starting from Eq.(28) we *raise* the power from  $-3 - \varepsilon/2$  to  $1 - \varepsilon/2$  and, successively, integrate by parts. Note that, for the massless pentagon the coefficient  $B$  becomes,

$$B = \frac{1}{16} s_{12} s_{23} s_{34} s_{45} s_{51}. \quad (30)$$

For the fully massive pentagon we derive, after four iterations of the BT-algorithm (from power  $-3 - \varepsilon/2$  to power  $1 - \varepsilon/2$ ), an expression which, remarkably enough, has no 4-dimensional integrals. In Tab. 1 we give the number of terms for the scalar box, pentagon and hexagon functions, where in all cases we have *raised* powers up to  $1 - \varepsilon/2$  and then we have expanded around  $\varepsilon = 0$  up to terms of  $\mathcal{O}(1)$ . Once more, the number of terms is not the relevant issue, only the smoothness of the integrand matters. No attempt has been performed, so far, towards a systematic study of the singularities (zeros of  $B$ ) of multi-leg,  $n \geq 5$ , one-loop diagrams.

### 2.1.3 Other one-loop infrared-divergent functions

One of the nice features of the method is that the coefficient  $B$  in Eq.(1) contains all divergences of the diagram, including the infrared pole, as discussed for the triangle one-loop diagram in Section 2.1.1. For other one-loop diagrams there is no need to have separate derivations for the infrared cases. All of them are reducible to  $C_0$ -functions. Typical example is the box diagram  $D_0$ , where we can use the following decomposition [9] (see also ref. [53]):

$$D_0 \left( -m_e^2, -m_e^2, -m_f^2, -m_f^2, Q^2, P^2; 0, m_e, 0, m_f \right) = \frac{1}{Q^2} \left[ -\bar{J}_{\gamma\gamma} \left( Q^2, P^2; m_e, m_f \right) \right]$$

diagram	5-dim	4-dim	3-dim	2-dim	1-dim	0-dim
$D_0$ Box	-	-	2	54	217	98
$E_0$ Pentagon	-	-	9	189	945	12826
$F_0$ Hexagon	1	44	693	4581	13860	228846

Table 1: Number of terms in scalar box, pentagon and hexagon functions where the BT-algorithm has been applied repeatedly up to powers  $1 - \varepsilon/2$ .

$$\begin{aligned}
& +C_0\left(-m_e^2, -m_f^2, P^2; m_e, 0, m_f\right) + C_0\left(-m_f^2, -m_e^2, P^2; m_f, 0, m_e\right)], \\
D_0\left(-m_e^2, -m_e^2, -m_f^2, -m_f^2, Q^2, P^2; 0, m_e, M_Z, m_f\right) &= \frac{1}{Q^2 + M_Z^2} \left[ -\bar{J}_{\gamma Z}\left(Q^2, P^2; m_e, m_f\right) \right. \\
& \left. -C_0\left(-m_e^2, -m_f^2, P^2; m_e, M_Z, m_f\right) + C_0\left(-m_f^2, -m_e^2, P^2; m_f, 0, m_e\right) \right], \\
D_0\left(-m_e^2, -m_e^2, -m_f^2, -m_f^2, Q^2, P^2; M_Z, m_e, 0, m_f\right) &= \frac{1}{Q^2 + M_Z^2} \left[ \bar{J}_{Z\gamma}\left(Q^2, P^2; m_e, m_f\right) \right. \\
& \left. +C_0\left(-m_e^2, -m_f^2, P^2; m_e, 0, m_f\right) - C_0\left(-m_f^2, -m_e^2, P^2; m_f, M_Z, m_e\right) \right].
\end{aligned}$$

All infrared divergent terms are contained in the  $C_0$ -functions and the additional integrals are as follows:

$$\begin{aligned}
i\pi^2 \bar{J}_{\gamma\gamma}\left(Q^2, P^2; m_e, m_f\right) &= \mu^{4-n} \int d^n q \frac{2q \cdot (q + Q)}{d_0(0) d_1(m_e) d_2(0) d_3(m_f)}, \\
i\pi^2 \bar{J}_{\gamma Z}\left(Q^2, P^2; m_e, m_f\right) &= \mu^{4-n} \int d^n q \frac{2q \cdot Q}{d_0(0) d_1(m_e) d_2(M_Z) d_3(m_f)}, \\
i\pi^2 \bar{J}_{Z\gamma}\left(Q^2, P^2; m_e, m_f\right) &= \mu^{4-n} \int d^n q \frac{2Q \cdot (q + Q)}{d_0(M_Z) d_1(m_e) d_2(0) d_3(m_f)},
\end{aligned} \tag{31}$$

The propagators are defined by

$$\begin{aligned}
d_0 &= q^2 + m_1^2 - i\delta, & d_1 &= (q + p_1)^2 + m_2^2 - i\delta, \\
d_2 &= (q + p_1 + p_2)^2 + m_3^2 - i\delta, & d_3 &= (q + p_1 + p_2 + p_3)^2 + m_4^2 - i\delta,
\end{aligned} \tag{32}$$

with all four-momenta flowing inwards and we have explicitly written the internal masses.

### 2.1.4 Reduction

The standard procedure in dealing with one-loop diagrams is based on the introduction of scalar functions,  $B_0, C_0$  etc, and of tensor integrals that are reduced to linear combinations of scalar ones [9]. The functional relation, Eq.(1), can be written in a more general form starting from

$$\int_S dx Q(x) \prod_i V_i^{\mu_i}(x), \quad (33)$$

where  $Q(x)$  is an arbitrary polynomial of  $x$ . Hence we are led to consider also the tensorial integrals in parametric space with no pre-reduction in momentum space and no appearance of standard Gram's determinants. Consider some simple example: we begin with the one-loop electron self-energy in QED, see Fig. 2,

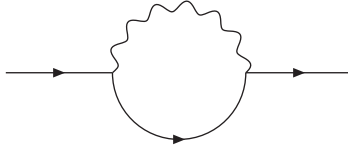


Figure 2: Fermionic self-energy in QED.

$$\begin{aligned} \Sigma &= -ie^2 \pi^{2-\epsilon/2} \mu^\epsilon \Gamma\left(\frac{\epsilon}{2}\right) \int_0^1 dx \left[ i(2-\epsilon) x \not{p} + (4-\epsilon) m_e \right] \chi^{-\epsilon/2}, \\ \chi(x) &= (1-x) \left( x p^2 + m_e^2 \right). \end{aligned} \quad (34)$$

After integration by parts we obtain

$$\begin{aligned} \Sigma &= -i\pi^2 e^2 \left[ \Sigma_p i \not{p} + \Sigma_m m_e \right], \\ \Sigma_p &= \frac{1}{\bar{\epsilon}} + \frac{p^2}{(p^2 + m_e^2)^2} \left[ \frac{\gamma}{2} \frac{(p^2 + m_e^2)^2}{p^2} - \frac{1}{3} m_e^2 - \frac{1}{6} p^2 \right. \\ &\quad \left. + \int_0^1 dx \left( \frac{1}{2} - \frac{1}{2} \frac{m_e^2}{p^2} - 4x \right) \chi \ln \frac{\chi}{\mu^2} \right], \\ \Sigma_m &= \frac{4}{\bar{\epsilon}} + \frac{p^2}{(p^2 + m_e^2)^2} \left[ \left( 2\gamma - \ln \frac{m_e^2}{\mu^2} + \frac{1}{2} \right) \frac{(p^2 + m_e^2)^2}{p^2} + p^2 \ln \frac{m_e^2}{\mu^2} - \frac{2}{3} p^2 \right. \\ &\quad \left. + m_e^2 \left( 3 \ln \frac{m_e^2}{\mu^2} - 2 \right) - 6 \int_0^1 dx \chi \ln \frac{\chi}{\mu^2} \right]. \end{aligned} \quad (35)$$

Note that the general idea is now different from the one which is at the basis of the analytical approach. The number of terms in the final expression does not matter and the only relevant

requisite is the smoothness of the integrand accompanied by the absence of high negative powers of true Gram's determinants in the reduction procedure. However, in this case a new and unpleasant feature shows up, namely the evaluation of the self-energy is numerical unstable at threshold,  $p^2 \approx -m_e^2$ .

Another example is given by the one-loop vertex of Fig. 3 which is reducible to the following expression:

$$\Lambda_\mu = -(2\pi)^4 i \frac{ie^3}{16\pi^2} \left[ \gamma_\mu V_1(Q^2; m, m) + \sigma_{\mu\nu} (p_1 + p_2)_\nu V_2(Q^2; m, m) \right]. \quad (36)$$

For  $V_1$  we obtain

$$\begin{aligned} V_1(Q^2; m, m) &= \pi^2 e^3 \int_0^1 dx \int_0^x dy \left\{ \left[ -2m_e^2 V_1^m - 2Q^2 V_1^q \right] \chi^{-1} - V_1^{\text{sing}} \right\}, \\ V_1^m &= x^2 + 3x - 3, \quad V_1^q = y^2 - xy + x - 1, \\ V_1^{\text{sing}} &= \frac{1}{2} (\epsilon - 2)^2 \left( \frac{1}{\bar{\epsilon}} - \ln \frac{\chi}{\mu^2} \right), \\ \chi(x, y) &= x^2 m_e^2 + y(x - y) Q^2. \end{aligned} \quad (37)$$

Note that we have already expanded in  $\epsilon$  because *raising* of powers can actually be done even in four dimensions. This new result can be derived by the following example: for  $\mu = -1 + \epsilon$  we write

$$\left[ 1 - \frac{(x + X) \partial_x}{2(\mu + 1)} \right] V^\epsilon = B V^{-1+\epsilon}, \quad (38)$$

and expand in  $\epsilon$  before integration by parts. By equating the coefficients of  $\epsilon^n$  we derive, for instance, that

$$B V^{-1} = 1 - \frac{1}{2} (x + X) \partial_x \ln V, \quad \text{etc}, \quad (39)$$

showing that we can expand first and then integrate by parts. A similar result can be derived with  $\mu = \epsilon$ , giving

$$B \ln V = V \ln V + \frac{1}{2} (x + X) \partial_x \left[ V (1 - \ln V) \right]. \quad (40)$$

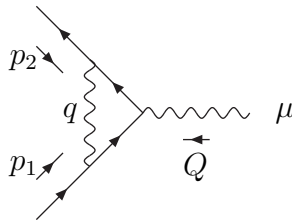


Figure 3: QED vertex diagram.

### 2.1.5 Zeros of $B$

The relation between the zeros of  $B$  and the Landau singularities for an arbitrary diagram  $G$  remains to be examined, although  $B = 0$  should contain all singularities of  $G$ . In this section we consider the one-loop three-point function and establish the result that the coefficient  $B$  emerging after the first application of Eq.(1) is connected with the leading Landau singularity, the so-called anomalous threshold. Moreover, a second iteration produces several coefficients that are connected with sub-leading singularities, i.e. those of the contracted diagrams. This result holds also for higher one-loop functions, although the determination of the explicit form of the anomalous thresholds is, in general, an arduous task.

Note that  $B$  is not a Gram determinant but its zeros are a vexation, as much as those of Gram determinants in the standard reduction procedure [9]. As already observed in ref. [50] the numerical advantage of smoother integrands is lost near thresholds where numerical convergence may become poor. This fact is best illustrated with a simple example, the scalar two point function,

$$B_0(-s; m, m) = \frac{1}{\varepsilon} - \ln \frac{m^2}{\mu^2} + 2 - \beta \ln \frac{\beta - 1}{\beta + 1}, \quad \beta^2 = 1 - 4 \frac{m^2}{s}. \quad (41)$$

The explicit result shows the well-known normal threshold at  $s = 4m^2$ . If we apply Eq.(1) the following result is obtained:

$$B_0(-s; m, m) = \pi^{-\epsilon/2} \mu^\epsilon \Gamma\left(\frac{\epsilon}{2}\right) \int_0^1 dx \chi^{-\epsilon/2} = \frac{4}{\beta^2} \pi^{-\epsilon/2} \mu^\epsilon \frac{\Gamma\left(\frac{\epsilon}{2}\right)}{\epsilon - 2} \left[ (3 - \epsilon) \right. \\ \left. \times \int_0^1 dx \chi^{1-\epsilon/2} - (m^2)^{1-\epsilon/2} \right], \quad (42)$$

with  $\chi = sx^2 - sx + m^2 - i\delta$ . Of course there is no pole at  $s = 4m^2$  but numerical convergence becomes questionable. An interesting question is related to the singularity of  $B_0$ . Can we find it without having to perform the integration? The integrand is  $\ln(x^2 - x + \mu^2)$  with  $\mu^2 = m^2/s$  and shows two branch points,  $x_\pm$ , that are complex conjugated below threshold and pinch the contour at  $x = 1/2$  when we are at threshold. We rewrite

$$\int_0^1 dx \ln \chi = -2 + \ln \mu^2 + \frac{1}{2} (4\mu^2 - 1) \int_0^1 dx \chi^{-1}. \quad (43)$$

The integrand will show poles at  $x_\pm$  and we are more familiar with the fact that two poles, pinching the integration contour, produce a singularity for the function [49]. In ref. [50] an alternative method is suggested to deal with regions near thresholds (see also ref. [54]), while our solution to the problem will be discussed in Section 3.1.4. Another example is represented by the triangle diagram. For the function

$$C_0(-m_a^2, -m_b^2, -s; m_b, M, m_a) \quad (44)$$

we obtain the explicit form of the  $\Delta$  factors of Eq.(14):

$$\Delta_1 = -\frac{1}{4} \lambda \left( s, m_a^2, m_b^2 \right), \quad \Delta_2 = -\frac{1}{4} \lambda \left( M^2, m_a^2, m_b^2 \right), \quad \Delta_3 = -\frac{1}{4} \lambda \left( M^2, m_a^2, m_b^2 \right), \quad (45)$$

that correspond to the three possible cuts of the triangle diagram,  $\lambda$  being the Källén function,

$$\lambda(x, y, z) = x^2 + y^2 + z^2 - 2(xy + xz + yz). \quad (46)$$

The zeros of  $\Delta_i$  correspond to non-leading Landau singularities, a) normal thresholds at  $s = (m_a + m_b)^2$  etc. and b) pseudo-thresholds at  $s = (m_a - m_b)^2$  etc. The latter do not show up in the physical Riemann sheet. Furthermore, we also derive

$$\Delta = \left[ (m_a^2 - m_b^2)^2 - M^2 s \right] \left[ s + M^2 - 2(m_a^2 + m_b^2) \right]. \quad (47)$$

For the special case  $m_a = m_b = m$  we get

$$\Delta = -M^2 s \left( s + M^2 - 4m^2 \right), \quad (48)$$

and  $s = 4m^2 - M^2$  corresponds to the leading Landau singularity, the anomalous threshold. Note that the general form of the leading Landau singularity is

$$s = \frac{1}{2m_2^2} \left\{ 2m_2^2(m_1^2 + m_3^2) - (m_1^2 + m_2^2 - M_1^2)(m_3^2 + m_2^2 - M_2^2) \pm \left[ \lambda(M_1^2, m_1^2, m_2^2) \lambda(M_2^2, m_3^2, m_2^2) \right]^{1/2} \right\}, \quad (49)$$

where we have introduced  $p_i^2 = -M_i^2$ .

For all the zeros of  $\Delta$  and  $\Delta_i$  numerical convergence is at stake. Here the method suffers the same disease of the usual appearance of Gram's determinants in the standard evaluation of  $C_0$  and in the reduction of vector and tensor triangles, although the origin of the phenomenon is rather different. Finally, consider the simple case where  $m_a = m_b = 0$ . The exact expression is

$$C_0(0, 0, -s; 0, M, 0) = -\frac{1}{s} \left[ \zeta(2) - \text{Li}_2 \left( 1 + \frac{s}{M^2} \right) \right], \quad (50)$$

where  $\zeta$  is the Riemann zeta-function and  $\text{Li}_2(z)$  is the standard di-logarithm. The zero of  $G_{11}$  is at  $s = 0$ , while  $G_2$  has two zeros, respectively at  $s = 0$  and  $s = -M^2$ . Note that there is no pole at  $s = 0$  in Eq.(50), that the function is regular at  $s = -M^2$  and that the only singularity is the branch point of the di-logarithm.

Actually these problems are easily solved in the standard approach. Consider the case of an arbitrary triangular graph for vanishing Gram's determinant:

$$C_0(p_1^2, p_2^2, Q^2; m_1, m_2, m_3) = C_0 = \sum_{n=0}^{\infty} C_{0n}(p_1^2, p_2^2, Q^2; m_1, m_2, m_3) \delta_3^n. \quad (51)$$

The kinematics for vanishing Gram's determinant,  $\Delta_3 \rightarrow 0$ , is as follows:

$$\begin{aligned}\Delta_3 &= p_1^2 p_2^2 - (p_1 \cdot p_2)^2 = \delta_3 P^4, \\ p_1^2 &= P^2, \quad p_2^2 = (\alpha_0^2 + \delta_3) P^2, \quad p_1 \cdot p_2 = -\alpha_0 P^2, \\ Q^2 &= -(p_1 + p_2)^2 = -[(1 - \alpha_0)^2 + \delta_3] P^2.\end{aligned}\tag{52}$$

In lowest order the solution is to introduce three different pinches of the basic three-point integral which correspond to the three ways of cutting the triangular graph:

$$C_{00}^{(1)} = B_0(23)|_{\delta_3=0}, \quad C_{00}^{(2)} = B_0(13)|_{\delta_3=0}, \quad C_{00}^{(3)} = B_0(12)|_{\delta_3=0}\tag{53}$$

Then a solution, free of singularities, is

$$\begin{aligned}C_{00} &= \frac{1}{N_0} \left[ -C_{00}^{(3)} + (1 - \alpha_0) C_{00}^{(2)} + \alpha_0 C_{00}^{(1)} \right], \\ N_0 &= m_2^2 - m_3^2 + (m_1^2 - m_2^2) \alpha_0 + P^2 \alpha_0 (1 - \alpha_0),\end{aligned}\tag{54}$$

where  $\alpha_0$  is given in Eq.(52). At next order we have 12 terms:

$$\begin{aligned}C_{01} &= \frac{2}{3} N_0^{-2} + \frac{1}{3} \Lambda N_0^{-3} C_{00} + N_0^{-2} C_{00} - \frac{2}{3} \frac{\mu_1^2}{1 - \alpha_0} N_0^{-2} A_0(1) \\ &\quad - \frac{2}{3} \frac{\mu_2^2}{\alpha_0} N_0^{-2} A_0(2) + \frac{2}{3} \beta_1 \mu_3^2 N_0^{-2} A_0(3) - \frac{1}{3} b_{12} N_0^{-2} C_{00}^{(2)} \\ &\quad - \frac{2}{3} \frac{1}{1 - \alpha_0} N_0^{-1} C_{00}^{(2)} + \frac{1}{3} a_{12} N_0^{-2} C_{00}^{(1)} - \frac{2}{3} \frac{1}{\alpha_0} N_0^{-1} C_{00}^{(2)} \\ &\quad + (1 - \alpha_0) N_0^{-1} C_{01}^{(2)} + \alpha_0 N_0^{-1} C_{01}^{(1)}.\end{aligned}\tag{55}$$

where we have introduced the following additional quantities:

$$\begin{aligned}m_i^2 &= -\mu_i^2 P^2, \quad b_{12} = 1 + \mu_1^2 - \mu_2^2, \quad a_{12}^2 = 4\mu_2^2 + \Lambda^2, \\ \Lambda^2 &= b_{12}^2 - 4\mu_1^2, \quad \beta_1 = \frac{1}{\alpha_0} + \frac{1}{1 - \alpha_0}.\end{aligned}\tag{56}$$

At second order we have an expression with 48 terms while 135 terms are needed at third order. For a general treatment of the reduction we refer to the work in ref. [55].

## 2.2 Multi-loop diagrams

In moving to multi-loop diagrams we recall that any diagram  $G$  with  $N_L$  legs and  $n_l$  loops is representable as [56]

$$G = (i \pi^{n/2})^{n_l} \Gamma \left( N_L - \frac{n}{2} n_l \right) \int \frac{dx_G \delta(1 - x_G)}{U^{n/2} (V - i\delta)^{N_L - n n_l/2}},\tag{57}$$

where  $\Gamma$  is the Euler gamma-function and where the integration measure can be written as

$$dx_G = \prod_{i=1}^{N_l} dx_i, \quad x_G = \sum_{i=1}^{N_l} x_i. \quad (58)$$

Furthermore, the polynomials  $V$  and  $U$  are defined by

$$\begin{aligned} V &= \sum_i m_i^2 x_i + \sum_i q_i^2 x_i - \frac{1}{U} \sum_{ij} B_{ij} q_i \cdot q_j x_i x_j, \\ U &= \sum_T \prod_{x_i \in T} x_i = \det(U_{rs}), \quad U_{rs} = \sum_i x_i \eta_{ir} \eta_{is}, \end{aligned} \quad (59)$$

where  $\eta_{is}$  is the projection of line  $i$  along the loop  $s$ . Furthermore,  $T$  is a co-tree and  $B_{ij}$  are the parametric functions for the given diagram. Although these functions can be determined completely by the topological structure of the diagram  $G$  we give a practical example of how to construct  $U$  and  $V$  for the two-loop diagram  $S_4$  of Fig. 4

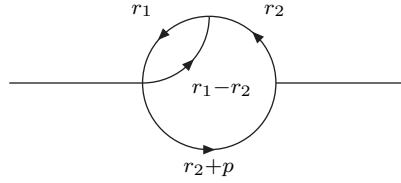


Figure 4: The two-loop diagram  $S_4$ . Arrows indicate the momentum flow.

After introducing Feynman parameters the integrand for  $S_4$  contains a factor  $1/D^4$  with

$$D = \sum_{i=1}^4 x_i (q_i^2 + m_i^2), \quad q_1 = r_1, \quad q_2 = r_1 - r_2, \quad q_3 = r_2, \quad q_4 = r_2 + p, \quad (60)$$

where  $r_s$  is the independent integration momentum around the loop  $s$ ,  $x_i$  are Feynman parameters with  $\sum_i x_i = 1$ . The part of  $D$  which is quadratic in  $r_{1,2}$  will be written as

$$r^t U r, \quad U_{11} = x_1 + x_2, \quad U_{22} = x_2 + x_3 + x_4, \quad U_{12} = U_{21} = -x_2. \quad (61)$$

Next we rewrite  $U_{ij}$  as a sum,

$$U_{ij} = \sum_{l=1}^4 \eta_{li} \eta_{lj} x_l, \quad (62)$$

and derive the coefficients  $\eta$  as

$$\eta_{11} = \eta_{21} = \eta_{32} = \eta_{42} = +1, \quad \eta_{22} = -1, \eta_{31} = \eta_{41} = \eta_{12} = 0. \quad (63)$$



Furthermore, let  $U$  be the determinant of the matrix  $U_{ij}$ , thus

$$U = \det (U_{ij}) = x_1 x_{234} + x_2 x_{34}, \quad (64)$$

where  $x_{ij\dots l} = x_i + x_j + \dots + x_l$ . Momenta  $p_i$  will then be defined with  $p_4 = p$  and  $p_i = 0$  for  $i < 4$ . The following change of variables in the  $r_1$ -integral is then performed:

$$r_1^\mu \rightarrow r_1^\mu - \sum_{j=1}^4 \sum_{t=1}^2 x_j p_4^\mu \eta_{jt} (U^{-1})_{1t} = r_1^\mu - \sum_{t=1}^2 x_4 p^\mu \eta_{4t} (U^{-1})_{1t} = r_1^\mu - x_4 \frac{x_2}{U} p^\mu. \quad (65)$$

Similarly we change variable also in the  $r_2$ -integral,

$$r_2^\mu \rightarrow \sum_{j=1}^4 \sum_{r=1}^2 x_j p_j^\mu \eta_{jr} (U^{-1})_{2r} = r_2^\mu - x_4 \frac{x_{12}}{U} p^\mu. \quad (66)$$

We derive the following result:

$$\sum_{i=1}^4 x_i (q_i^2 + m_i^2) \rightarrow r^t U r + V, \quad (67)$$

which defines the polynomial  $V$  as

$$V = \sum_{i=1}^4 x_i m_i^2 + x_4 p^2 - \frac{1}{U} x_{12} x_4^2 p^2. \quad (68)$$

After a diagonalization of the symmetric matrix  $U$ ,

$$\sum_{i'j'} (A^{-1})_{ii'} U_{i'j'} A_{j'j} = U_i \delta_{ij}, \quad (69)$$

we perform a change of variables with unit Jacobian,  $s_i = \sum_j A_{ij} r_j$ , and use

$$\begin{aligned} & \int \prod_{i=1}^{n_l} ds_i \left[ \sum_{i=1}^{n_l} U_i s_i^2 + V \right]^{-N_L} = \int \prod_{i=2}^{n_l} ds_i ds_1 \left[ U_1 s_1^2 + \sum_{i=2}^{n_l} U_i s_i^2 + V \right]^{-N_L} \\ & = i \pi^{n/2} U_1^{-n/2} \frac{\Gamma(N_L - n/2)}{\Gamma(N_L)} \int \prod_{i=2}^{n_l} ds_i \left[ \sum_{i=2}^{n_l} U_i s_i^2 + V \right]^{n/2 - N_L} = \text{etc.}, \end{aligned} \quad (70)$$

to obtain the result of Eq.(57). Similarly for the diagram  $S_3$  of Fig. 7 we derive

$$U = x_1 x_{23} + x_2 x_3, \quad V = \sum_{i=1}^4 x_i m_i^2 + \frac{1}{U} x_1 x_2 x_3 p^2. \quad (71)$$

Note that UV-singularities come from  $U$  so that, for finite diagrams, one should *raise* only the factor

$$\tilde{V} = U \left[ \sum_i m_i^2 x_i + \sum_i q_i^2 x_i \right] - \sum_{ij} B_{ij} q_i \cdot q_j x_i x_j. \quad (72)$$

There are several comments to be made before we can start trying to apply the BT-theorem to any multi-loop diagram. For two-loop diagrams  $U$  is a quadratic form in the Feynman parameters  $x$  and  $\tilde{V}$  is a cubic, so that we have to construct a BT functional relation for a quintic or higher polynomial. For  $N_L = 3, 4$ , we have that the corresponding diagram is defined to consist of  $\tilde{V}$  to a positive power and, in principle, it is enough to regularize  $G$  with some  $K_S$  operation ( $S \in G$ ) [56]. For  $N_L > 5$ , we have that the diagrams contains  $\tilde{V}$  to a negative power,  $U$  to a positive power. Therefore, there is no UV-divergency and we could *raise* the power for the cubic.

For self-energies at zero external momentum,  $p^2 = 0$ , the procedure is quite straightforward. Consider, for example, the case  $n_l = 2, N_L = 3$ . First of all, we perform a projective transformation [58]

$$x_i = A_i u_i / \sum_j A_j u_j, \quad A_i = \frac{1}{m_i^2}, \quad (73)$$

to obtain  $\tilde{V} = U$ , where  $U$  is a quadratic form. The important point being that we know how to *raise* powers for any quadratic form.

Finally,  $N_L = 2(n_l + 1)$  is a nice example of a single polynomial of degree  $n_l + 1$ . Of course, vacuum diagrams are also easy. At two-loop level we have only the diagram of Fig. 5 which becomes

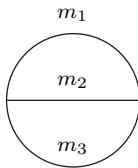


Figure 5: The two-loop vacuum diagram with arbitrary masses.

$$G_2^{\text{vac}} = (4\pi)^{\varepsilon-4} \mu^\varepsilon \Gamma(\varepsilon-1) \left(K^t H^{-1} K\right)^{-2} \int_0^1 dx \int_0^x dy \\ \times \left[1 - \frac{(x + K^t H^{-1}) \partial}{\varepsilon - 2}\right] \left[1 - \frac{(x + K^t H^{-1}) \partial}{\varepsilon}\right] U^{\varepsilon/2}(x, y), \quad (74)$$

where  $U$  can easily be derived according to the general rules presented above. The same is obviously true for tadpoles. All of this, however, still does not represent a real multi-loop application of the BT-theorem.

Additional problems are represented by the fact that  $\tilde{V}$  is an highly incomplete polynomial with few non-zero coefficients.  $\mathcal{P}$  can be found via a direct study of linear systems of  $n$  equations (usually,  $n \gg 100$ ) in  $m$  variables and very often the matrix of coefficients has rank  $< n$ , so the

system is generally impossible and we need to go to higher values of  $n, m$ , i.e. beyond  $n_{\min} = \min\{n < m\}$ . A simple counting shows the following situation: given a compact representation for  $\mathcal{P}$ ,

$$\mathcal{P} = P_n + P_{n+1}^i \partial_i + P_{n+2}^{ij} \partial_i \partial_j + \dots \quad (75)$$

four variables and a cubic  $V$  require  $n_{\text{eq}} = 126(330, 715)$  and  $n_{\text{var}} = 155(415, 871)$  for  $n = 2(1, 0)$  and first(second, third) derivatives. Simple examples already show that, for realistic polynomials  $V$ , one has to go beyond second order in derivatives.

### 3 A minimal BT approach

The original proposal by F. V. Thachov requires knowledge of the polynomial  $\mathcal{P}$  of Eq.(1), iterative application of the functional relation Eq.(1) followed by integration by parts. After a Laurent expansion in  $\epsilon = 4 - n$  one can achieve an arbitrary degree of smoothness of the integrand. In principle, the denominators  $B$  will contain thousands of terms and may lead to large numerical instabilities around thresholds.

We have not been able to derive any compact form for the polynomial  $\mathcal{P}$  of Eq.(1), even for the simplest two-loop topology. Instead, we have adopted a different strategy aimed to deal with arbitrary two-loop diagrams. It represents a compromise based on the simple observation that we know how to apply the BT-iterative procedure for arbitrary one-loop diagrams. Therefore, given any two-loop diagram  $G$  (for an illustration see Fig. 6) we apply the BT functional relation to  $G_L$ , the one-loop sub-diagram of  $G$  which has the largest number of internal lines. In this way the integrand for  $G$  in  $x$ -space can be made smooth, a part from the factor  $B$  of Eq.(1) which is now a polynomial in  $x_s$ , the Feynman parameters needed for the complementary sub-diagram of  $G$  with the smallest number of internal lines,  $G_S$ . The sub-diagram  $G_S$ , after integration over its momentum, becomes an additional  $-x_s$ -dependent and with non-canonical power  $-$  propagator for  $G_L$ .

This procedure can be immediately generalized to any number of loops. Furthermore, one should realize that the BT procedure does not introduce singularities through  $B(x_s)$ , a part from the singularities in the external parameters of the original diagram. Therefore, before performing the  $x_s$ -integration we move the integration contour into the complex hyper-plane, thus avoiding the crossing of apparent singularities. The idea of distorting the contour has been introduced in [59] and we have modified it to deal with the  $x_s$ -integration.

A complete study of two-loop two-point functions (self-energies) has shown [57] that, for one iteration, a transformation of the corresponding Feynman parameters can always be found that produces a coefficient  $B$  which is  $x_s$ -independent. In this way we are able to avoid distortion of the integration contour. However, this coefficient  $B$  will vanish at some non-leading Landau singularity of the diagram where additional analytical work is needed before starting the numerical evaluation. A detailed derivation will be given in [57].

In the following section we present a simple example that illustrates all the features connected with integration in complex parametric space.

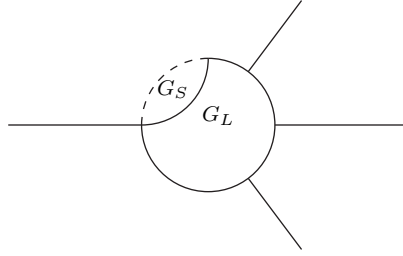


Figure 6: A generic two-loop diagram  $G$ ; internal solid lines give the largest sub-diagram  $G_L$ .

### 3.0.1 An example

An instructive example is the following: suppose that we have to compute

$$I = \int_0^1 dx B_0(-s; xm, m), \quad (76)$$

where  $B_0$  is the scalar, one-loop, two-point function. Suppose also that we have no analytical expression available for  $B_0$  which, of course, we have but, nevertheless, let us assume that we do not. The integral of Eq.(76) becomes

$$I = i \pi^{2-\epsilon/2} \Gamma\left(\frac{\epsilon}{2}\right) \int_0^1 dx \int_0^1 dy \chi^{-\epsilon/2}, \quad (77)$$

$$\chi(x, y) = s y^2 - (s - m^2 + x^2 m^2) + x^2 m^2 - i \delta,$$

with  $\delta \rightarrow 0_+$ . Then Eq.(4) applies for

$$B = -\frac{1}{4s} \lambda(s, x^2 m^2, m^2), \quad Y = -\frac{1}{2s} (s - m^2 + x^2 m^2), \quad (78)$$

with the following result:

$$\int_0^1 dy \chi^{-\epsilon/2} = -4 \frac{s}{\lambda} \int_0^1 dy \left[ 1 - \frac{1}{2-\epsilon} (y + Y) \frac{\partial}{\partial y} \right] \chi^{1-\epsilon/2}. \quad (79)$$

After integration by parts we obtain

$$\int_0^1 dy \chi^{-\epsilon/2} = -4 \frac{s}{\lambda} \frac{1}{2-\epsilon} \left[ (3-\epsilon) \int_0^1 dy \chi^{1-\epsilon/2} - (1+Y) (m^2)^{1-\epsilon/2} + Y (x^2 m^2)^{1-\epsilon/2} \right]. \quad (80)$$

This strategy is dubious if the roots of  $\lambda = 0$  are inside the interval  $[0, 1]$ , on the real axis. These roots are easily evaluated and are given by

$$x_{\pm}^{\pm} = \frac{1 \pm \mu}{\mu}, \quad x_{\pm}^{\mp} = -\frac{1 \pm \mu}{\mu}, \quad \mu^2 s = m^2. \quad (81)$$

Therefore

$$x = \frac{\mu - 1}{\mu}, \quad \text{for } \mu > 1, \quad x = \frac{1 - \mu}{\mu}, \quad \text{for } \mu < \frac{1}{2}, \quad (82)$$

are the apparent singularities in the interval  $[0, 1]$ . Crossing of these points is avoided by moving the  $x$ -integration into the complex plane. How to deform the integration path is suggested by simple considerations: take the quadratic form  $\chi$  of Eq.(77); as a function of  $x$  there are two roots,

$$\chi(x, y) = \mu^2 (1 - y) (x + x_0 + i \delta) (x - x_0 - i \delta), \quad x_0^2 = \frac{(1 - \mu^2)y - y^2}{\mu^2(1 - y)}. \quad (83)$$

Therefore, for  $1 - \mu^2 \leq y \leq 1$  we have two branch points at  $\pm i|x_0|$ . Instead, for  $0 \leq y \leq 1 - \mu^2$  the branch points are real and  $\chi \leq 0$  for  $0 \leq x \leq x_0$ . Furthermore,  $x_0 \leq 1$  for  $y \leq y_-$  or  $y \geq y_+$  with  $y_{\pm} = (1 \pm \beta)/2$  and  $\beta^2 = 1 - 4\mu^2$ . Thanks to the infinitesimal imaginary parts we have

$$\ln \chi = \ln \mu^2 + \ln (1 - y) + \ln (x + x_0 + i \delta) + \ln (x - x_0 - i \delta), \quad (84)$$

and only the last logarithm contributes to the imaginary part. To avoid crossing the cut of the logarithm ( $[-\infty, x_0]$ ) we choose any smooth curve connecting  $x = 0$  to  $x = 1$  in the  $x$  lower half-plane. By comparing two expressions for  $I$  (as defined in Eq.(76)), the first computed from the known analytical result for the  $B_0$ -function and a second one obtained through the double-integral originating from Eq.(80) we find agreement in 8-digits, as shown in Tab. 2.

$\sqrt{s}$ [GeV]	Eq.(76)	Eq.(80)
1.1	1.12256370(1) + $i$ 0.042810523(5)	1.12256370(1) + $i$ 0.042810523(11)
10	-2.52793882(1) + $i$ 3.09949189(0)	-2.52793882(3) + $i$ 3.09949189(3)
100	-7.20895671(4) + $i$ 3.14117375(0)	-7.20895671(7) + $i$ 3.14117375(7)

Table 2:  $I$  from Eq.(76) or Eq.(80) with  $m = 1$ .

### 3.1 The $S_3$ or sunset topology

After some preliminar considerations we are ready to start with a realistic example. Consider the simplest two-loop, two-point topology with three internal lines, the so-called sunset diagram illustrated in Fig. 7. Literature relevant to the sunset (sunrise) topology is assembled, for convenience, in ref. [48]. The corresponding integral will be

$$\pi^4 S_3 = \mu^{2\epsilon} \int d^n q_1 d^n q_2 (q_1^2 + m_1^2)^{-1} \left( (q_1 - q_2 + p)^2 + m_2^2 \right)^{-1} (q_2^2 + m_3^2)^{-1}. \quad (85)$$

Here we introduce a special notation,  $(\alpha, m_1 | \gamma, m_2, p | \beta, m_3)$ , for

$$\mu^{2\epsilon} \int d^n q_1 d^n q_2 (q_1^2 + m_1^2)^{-\alpha} \left( (q_1 - q_2 + p)^2 + m_2^2 \right)^{-\gamma} (q_2^2 + m_3^2)^{-\beta}, \quad (86)$$

and  $(\mu_1 \dots \mu_i \mid \nu_1 \dots \nu_j \mid \alpha, m_1 \mid \gamma, m_2, p \mid \beta, m_3)$  for

$$\mu^{2\epsilon} \int d^n q_1 d^n q_2 q_1^{\mu_1} \dots q_1^{\mu_i} q_2^{\nu_1} \dots q_2^{\nu_j} (q_1^2 + m_1^2)^{-\alpha} \left( (q_1 - q_2 + p)^2 + m_2^2 \right)^{-\gamma} (q_2^2 + m_3^2)^{-\beta}. \quad (87)$$

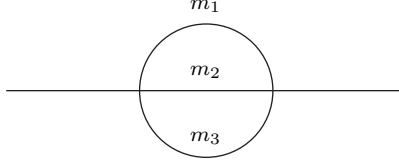


Figure 7: The  $S_3$  topology for two-loop self-energy diagrams.

The best way of dealing with the sunset integral is to introduce the so-called  $(\alpha\beta\gamma)$  partial integration [58] to obtain

$$S_3 = \sum_{i=1}^3 m_i^2 S_{3i} + S_{3p}. \quad (88)$$

With a suitable change of variables the four functions of Eq.(85) can be cast into the following form:

$$\begin{aligned} \pi^4 S_{31} &= \frac{\mu^{2\epsilon}}{\epsilon - 1} \int d^n q_1 d^n q_2 (q_1^2 + m_3^2)^{-1} \left( (q_1 - q_2 - p)^2 + m_2^2 \right)^{-1} (q_2^2 + m_1^2)^{-2} \\ &= (\epsilon - 1)^{-1} (1, m_3 \mid 1, m_2, -p \mid 2, m_1), \\ \pi^4 S_{32} &= \frac{\mu^{2\epsilon}}{\epsilon - 1} \int d^n q_1 d^n q_2 (q_1^2 + m_1^2)^{-1} \left( (q_1 - q_2 + p)^2 + m_3^2 \right)^{-1} (q_2^2 + m_2^2)^{-2} \\ &= (\epsilon - 1)^{-1} (1, m_1 \mid 1, m_3, p \mid 2, m_2), \\ \pi^4 S_{33} &= \frac{\mu^{2\epsilon}}{\epsilon - 1} \int d^n q_1 d^n q_2 (q_1^2 + m_1^2)^{-1} \left( (q_1 - q_2 + p)^2 + m_2^2 \right)^{-1} (q_2^2 + m_3^2)^{-2} \\ &= (\epsilon - 1)^{-1} (1, m_1 \mid 1, m_3, p \mid 2, m_2), \\ \pi^4 S_{3p} &= \frac{\mu^{2\epsilon}}{\epsilon - 1} \int d^n q_1 d^n q_2 q_2 \cdot p (q_1^2 + m_1^2)^{-1} \left( (q_1 - q_2 + p)^2 + m_3^2 \right)^{-1} (q_2^2 + m_2^2)^{-2} \\ &= (\epsilon - 1)^{-1} (0 \mid p \mid 1, m_1 \mid 1, m_3, p \mid 2, m_2), \end{aligned} \quad (89)$$

where, as usual,  $n = 4 - \epsilon$ . Their evaluation is discussed in Section 3.1.2 and in Section 3.1.3.

### 3.1.1 Landau equations for $S_{33}$

Before starting the evaluation of the sunset diagram it is important to know as much as possible about its singularities as a function of  $p^2$  and of the internal masses. The corresponding Landau equations are

$$\alpha_1 (q_1^2 + m_1^2) = 0, \quad \alpha_2 ((q_1 - q_2 + p)^2 + m_2^2) = 0, \quad \alpha_3 (q_2^2 + m_3^2) = 0, \quad (90)$$

and also

$$\alpha_1 q_{1\mu} + \alpha_2 (q_1 - q_2 + p)_\mu = 0, \quad -\alpha_2 (q_1 - q_2 + p)_\mu + \alpha_3 q_{2\mu} = 0. \quad (91)$$

The leading Landau singularity occurs for  $\alpha_i \neq 0, \forall i$ . We multiply the two equations Eq.(91) by  $q_{1\mu}, q_{2\mu}$  and  $p_\mu$  respectively. This gives an homogeneous system of six equations. If all  $\alpha_i$  are different from zero, the singularity will occur for

$$q_1^2 = -m_1^2, \quad q_2^2 = -m_3^2, \quad q_1 \cdot q_2 = \frac{1}{2} [m_2^2 - m_1^2 - m_3^2 - s + 2p \cdot (q_1 - q_2)]. \quad (92)$$

The Landau equations become as follows:

$$\begin{aligned} -m_1^2 \alpha_1 + [q_2 \cdot p + \frac{1}{2}(s - m_1^2 - m_2^2 + m_3^2)] \alpha_2 &= 0, \\ [q_1 \cdot p - q_2 \cdot p - \frac{1}{2}(s + m_1^2 - m_2^2 + m_3^2)] \alpha_1 + [q_1 \cdot p - \frac{1}{2}(s + m_1^2 - m_2^2 - m_3^2)] \alpha_2 &= 0, \\ q_1 \cdot p \alpha_1 + (-s + q_1 \cdot p - q_2 \cdot p) \alpha_2 &= 0, \\ [-q_2 \cdot p - \frac{1}{2}(s - m_1^2 - m_2^2 + m_3^2)] \alpha_2 + [q_1 \cdot p - q_2 \cdot p - \frac{1}{2}(s + m_1^2 - m_2^2 + m_3^2)] \alpha_3 &= 0, \\ [-q_1 \cdot p + \frac{1}{2}(s + m_1^2 - m_2^2 - m_3^2)] \alpha_2 - m_3^2 \alpha_3 &= 0, \\ (s - q_1 \cdot p + q_2 \cdot p) \alpha_2 + q_2 \cdot p \alpha_3 &= 0. \end{aligned} \quad (93)$$

There are two compatibility conditions for the first three equations that can be used to get  $q_1 \cdot p$  and  $q_2 \cdot p$ ,

$$q_1 \cdot p = \frac{m_1}{2} \frac{s - m_3^2 + (m_1 + m_2)^2}{m_1 + m_2}, \quad q_2 \cdot p = -\frac{1}{2} [s + m_3^2 - (m_1 + m_2)^2]. \quad (94)$$

Inserting these solutions into Eq.(93) we obtain that

$$\alpha_1 = \frac{m_2}{m_1} \alpha_2, \quad \alpha_3 = \frac{1}{2} \frac{m_2}{m_2^3} \left( \frac{s - m_3^2}{m_1 + m_2} - m_1 - m_2 \right) \alpha_2, \quad (95)$$

is a solution of the original system if and only if

$$s = (m_1 + m_2 \pm m_3)^2. \quad (96)$$

These are the leading singularities (plus permutations of masses), referred to as normal and pseudo thresholds. Note that pseudo-threshold does not correspond to a singularity on the physical Riemann sheet.

### 3.1.2 Evaluation of $S_{3i}$

We will now compute  $S_{33}$ , as given in Eq.(89), and the remaining  $S_{3i}$ -terms will follow from  $S_{33}$  with the corresponding permutations:

$$\begin{aligned} 31 & \text{ with } m_1 \leftrightarrow m_3, \quad p \leftrightarrow -p, \\ 32 & \text{ with } m_2 \leftrightarrow m_3. \end{aligned} \quad (97)$$

First a Feynman parameter  $x$  is introduced, and the  $q_1$ -integration is performed giving

$$\begin{aligned} S_{33} &= i \pi^{-2-\epsilon/2} \frac{\mu^{2\epsilon}}{\epsilon-1} \Gamma\left(\frac{\epsilon}{2}\right) \int_0^1 dx \int d^n q \left(q^2 + m_3^2\right)^{-2} \\ &\times \left[x(1-x)(q-p)^2 + xm_2^2 + (1-x)m_1^2\right]^{-\epsilon/2}, \end{aligned} \quad (98)$$

where we have introduced the Euler  $\Gamma$ -function. Next we change integration variable,  $q' = q - p$ , and introduce a  $x$ -dependent mass,

$$m_x^2 = \frac{(1-x)m_1^2 + xm_2^2}{x(1-x)}. \quad (99)$$

$S_{33}$  can be cast into the following form:

$$S_{33} = i \pi^{-2-\epsilon/2} \frac{\mu^{2\epsilon}}{\epsilon-1} \Gamma\left(\frac{\epsilon}{2}\right) \int_0^1 dx \left[x(1-x)\right]^{-\epsilon/2} \int d^n q \frac{q^2 + m_x^2}{(q^2 + m_x^2)^{1+\epsilon/2} \left((q+p)^2 + m_3^2\right)^2}. \quad (100)$$

According to some standard procedure we introduce a new Feynman parameter  $y$  and write

$$\begin{aligned} S_{33} &= i \pi^{-2-\epsilon/2} \frac{\mu^{2\epsilon}}{\epsilon-1} \Gamma\left(\frac{\epsilon}{2}\right) \int_0^1 dx \int_0^1 dy \left[x(1-x)\right]^{-\epsilon/2} (1-y)^{\epsilon/2} y \\ &\times \int d^n q \left(q^2 + m_x^2\right) \left[q^2 + 2yp \cdot q + y(p^2 + m_3^2) + (1-y)m_x^2\right]^{-3-\epsilon/2}. \end{aligned} \quad (101)$$

Let  $U$  be defined by

$$U = y(1-y)p^2 + ym_3^2 + (1-y)m_x^2 - i\delta, \quad (102)$$

with  $\delta \rightarrow 0_+$ , then  $S_{33}$  becomes

$$\begin{aligned} S_{33} &= -\pi^{-\epsilon} \frac{\mu^{2\epsilon}}{\epsilon-1} \frac{\Gamma(\epsilon/2)}{\Gamma(1+\epsilon/2)} \int_0^1 dx \int_0^1 dy \left[x(1-x)\right]^{-\epsilon/2} (1-y)^{\epsilon/2} \\ &\times y \left[\Gamma(1+\epsilon) \left(y^2 p^2 + m_x^2\right) U^{-1-\epsilon} + \left(2 - \frac{\epsilon}{2}\right) \Gamma(\epsilon) U^{-\epsilon}\right]. \end{aligned} \quad (103)$$

Next we introduce the Mandelstam variable  $s$ ,

$$p^2 = -s, \quad \mu_i^2 = \frac{m_i^2}{s}, \quad (104)$$



and scale  $U$  accordingly:

$$U = s \chi, \quad \chi = -y (1 - y) + \mu_3^2 y + \mu_x^2 (1 - y) - i \delta. \quad (105)$$

For the rest of this discussion we assume that  $s > 0$  and will postpone to Appendix B the discussion of the case  $s < 0$ .

There is no need to evaluate numerically the poles at  $\epsilon = 0 (n = 4)$ . We perform a Laurent expansion of the integrand around  $\epsilon = 0$ , after which the double pole is easy to compute and gives

$$\frac{2}{\epsilon^2} + \Delta_{UV}^2, \quad \Delta_{UV} = \gamma + \ln \pi + \ln \frac{s}{\mu^2}. \quad (106)$$

In this result  $\gamma = 0.577216$  is the Euler's constant and we have included in the definition of *double-pole* a bunch of constants. Also the single pole at  $\epsilon = 0 (n = 4)$  can be computed analytically. The  $x - y$  integration is greatly simplified by the use of the following relation:

$$\frac{\mu_x^2 - y^2}{\chi} = 1 - \frac{y}{\chi} \frac{\partial}{\partial y} \chi. \quad (107)$$

With the help of Eq.(107) we find the following result for the single-pole:

$$- \frac{2}{\epsilon} \Delta_{UV} + \left( 2 \ln \mu_3^2 - 3 \right) \left( \Delta_{UV} - \frac{1}{\epsilon} \right), \quad (108)$$

where, again, a bunch of constants have been included into the definition of *single-pole*. A detailed derivation is presented in Appendix A. Continuing our calculation we write

$$\begin{aligned} S_{33} = & - \frac{\pi^{-\epsilon}}{\epsilon - 1} \frac{\Gamma(\epsilon/2)}{\Gamma(1 + \epsilon/2)} \left( \frac{s}{\mu^2} \right)^{-\epsilon} \int_0^1 dx \int_0^1 dy \left[ x(1-x) \right]^{-\epsilon/2} (1-y)^{\epsilon/2} y \\ & \times \left[ \Gamma(1 + \epsilon) \left( -y^2 + \mu_x^2 \right) \chi^{-1-\epsilon} + \left( 2 - \frac{\epsilon}{2} \right) \Gamma(\epsilon) \chi^{-\epsilon} \right]. \end{aligned} \quad (109)$$

The quadratic form  $\chi$  is defined by

$$\chi = H y^2 + 2 K y + L, \quad (110)$$

with coefficients

$$H = 1, \quad K = -\frac{1}{2} \left( 1 - \mu_3^2 + \mu_x^2 \right), \quad L = \mu_x^2. \quad (111)$$

Our strategy will be to single out the  $y$ -integral and to *raise* the power of  $\chi$ . The coefficients relevant for this case are:

$$\begin{aligned} B = & \mu_x^2 - \frac{1}{4} \left( 1 - \mu_3^2 + \mu_x^2 \right)^2 = -\frac{1}{4} \lambda \left( 1, \mu_3^2, \mu_x^2 \right), \\ Y = & -\frac{1}{2} \left( 1 - \mu_3^2 + \mu_x^2 \right), \quad \mu = -1 - \epsilon, \end{aligned} \quad (112)$$

where  $\lambda$  is the usual Källén function. Therefore we obtain

$$\chi^{-1-\epsilon} = -\frac{4}{\lambda(1, \mu_3^2, \mu_x^2)} \left[ 1 + \frac{1}{2\epsilon} (y+Y) \frac{\partial}{\partial y} \right] \chi^{-\epsilon}. \quad (113)$$

No spurious singularity at  $\epsilon = 0$  is introduced in the r.h.s. of Eq.(113) and to avoid apparent poles we use a new variant of the basic functional relation, Eq.(1):

$$\chi^{-1-\epsilon} = -\frac{4}{\lambda(1, \mu_3^2, \mu_x^2)} \left\{ 1 - \frac{1}{2} (y+Y) \frac{\partial}{\partial y} \ln \chi - \epsilon \left[ \ln \chi - \frac{\epsilon}{4} (y+Y) \frac{\partial}{\partial y} \ln^2 \chi + \mathcal{O}(\epsilon^2) \right] \right\}. \quad (114)$$

Note that no new singularity in the variable  $x$  is introduced by the procedure. However, numerical instabilities could be introduced in the  $x$ -integration, especially if the process of *raising* powers is continued, resulting in a final expression with higher and higher negative powers of  $\lambda$ . For this reason we are led to study the zeros of the Källén function, i.e.  $\lambda(1, \mu_3^2, \mu_x^2) = 0$ . Clearly, if  $s < 0$  there are no real solutions for  $x$ . Otherwise solutions are given by

$$\left( \mu_x^2 \right)_{\pm} = (1 \pm \mu_3)^2. \quad (115)$$

Consider now  $\mu_x^2$  as a function of the variable  $x$ ,

$$\mu_x^2 = \frac{(1-x)\mu_1^2 + x\mu_2^2}{x(1-x)}. \quad (116)$$

The minimum, for  $\mu_x^2$ , occurs at  $x_{\pm} = \mu_1/(\mu_2 \pm \mu_1)$ . Only  $x_+$  lies between 0 and 1, corresponding to

$$\left( \mu_x^2 \right)_{\min} = (\mu_1 + \mu_2)^2. \quad (117)$$

There are three distinct possibilities:

1. the root  $(\mu_x^2)_+$  is below the minimum, i.e.  $\mu_1 + \mu_2 - \mu_3 \geq 1$ , therefore  $\lambda$  can never be zero.
2. Only one root is above the minimum, i.e.  $(1 - \mu_3)^2 \leq (\mu_1 + \mu_2)^2 \leq (1 + \mu_3)^2$ , when there are two values of  $x$  where  $\lambda = 0$ ,

$$x_{\pm}^{\pm} = \frac{1}{2(1 + \mu_3)^2} \left[ (1 + \mu_3)^2 + \mu_1^2 - \mu_2^2 \pm \lambda^{1/2} \left( (1 + \mu_3)^2, \mu_1^2, \mu_2^2 \right) \right]. \quad (118)$$

3. Both roots are above the minimum, i.e.  $(\mu_1 + \mu_2)^2 \leq (1 - \mu_3)^2$ , when we have four values of  $x$  where  $\lambda = 0$ . The new pair of points is given by

$$x_{\pm}^{\pm} = \frac{1}{2(1 - \mu_3)^2} \left[ (1 - \mu_3)^2 + \mu_1^2 - \mu_2^2 \pm \lambda^{1/2} \left( (1 - \mu_3)^2, \mu_1^2, \mu_2^2 \right) \right]. \quad (119)$$

For the finite part of this Feynman diagram we have now to understand when and where the imaginary part develops. Let us assume that  $s > 0$ . Imaginary parts are present as soon as  $\chi < 0$ . There are two solutions for  $y$  to the equation  $\chi = 0$ ,

$$y_{\pm} = \frac{1}{2} \left[ 1 - \mu_3^2 + \mu_x^2 \pm \lambda^{1/2} \left( 1, \mu_3^2, \mu_x^2 \right) \right]. \quad (120)$$

Therefore,  $\ln \chi$  develops an imaginary part for  $y_- \leq y \leq y_+$ , if and only if  $\lambda(1, \mu_3^2, \mu_x^2) > 0$ . As before, there are only three possibilities,

1.  $(1 + \mu_3^2)^2 \leq (\mu_1 + \mu_2)^2$ , where  $\lambda$  is always positive,
2.  $(1 - \mu_3^2)^2 \leq (\mu_1 + \mu_2)^2 \leq (1 + \mu_3^2)^2$ , where we have two alternatives,

$$\begin{aligned} (\mu_1 + \mu_2)^2 \leq \mu_x^2 \leq (1 + \mu_3^2)^2, & \quad \lambda \text{ is negative,} \\ \mu_x^2 \geq (1 + \mu_3^2)^2, & \quad \lambda \text{ is positive,} \end{aligned} \quad (121)$$

3.  $(\mu_1 + \mu_2)^2 \leq (1 - \mu_3^2)^2$  where we have three alternatives,

$$\begin{aligned} (\mu_1 + \mu_2)^2 \leq \mu_x^2 \leq (1 - \mu_3^2)^2, & \quad \lambda \text{ is positive,} \\ (1 - \mu_3^2)^2 \leq \mu_x^2 \leq (1 + \mu_3^2)^2, & \quad \lambda \text{ is negative,} \\ \mu_x^2 \geq (1 + \mu_3^2)^2, & \quad \lambda \text{ is positive,} \end{aligned} \quad (122)$$

Consider the original integral, Eq.(109); the integration hyper-contour can be distorted away from its original real location and when the possibility of this distortion ceases, we encounter a singularity of the function [49]. The difficulty in locating the singularities lies in imagining what happens in the multi-dimensional (complex) space of integration. In the case of Eq.(109) the integrand shows poles at the zeros of  $\chi(x, y)$ , i.e. for  $y = y_{\pm}(x)$  with  $y_{\pm}$  given in Eq.(120). We may distort the interval  $y \in [0, 1]$  but a pinch may appear for  $y_+ = y_-$ , which requires  $\lambda(1, \mu_3^2, \mu_x^2) = 0$ . Again, we can move the  $x$ -integration contour to avoid the points where this happens, i.e. for  $\mu_x^2 = (1 \pm \mu_3)^2$ ,

$$\mu_x^2 = (1 \pm \mu_3)^2, \quad \text{for } x = x_{\pm}^{\pm}. \quad (123)$$

However, if  $x_+^+ = x_-^+$  or  $x_+^- = x_-^-$  a singularity may appear. Note that for  $\mu_x^2 = (1 + \mu_3)^2$  we will have

$$y_{\pm} = 1 + \mu_3, \quad \chi = (y - 1 - \mu_3)^2, \quad (124)$$

while for  $\mu_x^2 = (1 - \mu_3)^2$  we have

$$y_{\pm} = 1 - \mu_3, \quad \chi = (y - 1 + \mu_3)^2, \quad (125)$$

so that, in the first case, the pinch should correspond to  $y > 1$ , therefore there is no singularity. In this case we will speak of the so-called pseudo-threshold, corresponding to  $s = (m_1 + m_2 - m_3)^2$ .

It is a well known fact that the  $S_3$  topology is regular at any of the pseudo-thresholds. On the contrary, when  $\mu_x^2 \rightarrow (1 - \mu_3)^2$  (or  $x \rightarrow x_{\pm}^-$ ) we have  $y_+ \rightarrow y_-$  from opposite sides of the integration contour but the relevant part of the integrand is  $(\mu_x^2 - y^2)/\chi$  which, for  $y = 1 - \mu_3 + \Delta$  ( $\Delta \rightarrow 0$ ) and  $\mu_x^2 = (1 - \mu_3)^2$  behaves as

$$\frac{\mu_x^2 - y^2}{\chi} \sim \frac{2(1 - \mu_3)\Delta}{\Delta^2 - i\delta}. \quad (126)$$

Therefore there is no pinch, even in this situation. Note that the condition  $x_+^- = x_-^-$  corresponds to the so-called normal threshold,  $s = (m_1 + m_2 + m_3)^2$  which is, nevertheless, a singular point of the sunset diagram. The singularity clearly arises from the remaining  $\chi^{-\epsilon}$  terms of the integrand, in the same way as the normal threshold singularity arises in the one-loop self-energy. This rather long discussion has been introduced for one specific purpose: if we rewrite  $S_{33}$  as

$$S_{33} = -\frac{\pi^{-\epsilon}}{\epsilon - 1} \frac{\Gamma(\epsilon/2)\Gamma(\epsilon)}{\Gamma(1 + \epsilon/2)} \left(\frac{s}{\mu^2}\right)^{-\epsilon} \int_0^1 dx \mathcal{S}_{33}(\epsilon, x), \quad (127)$$

then  $\mathcal{S}_{33}(\epsilon, x)$  has no poles at  $x = x_{\pm}^-$ . In other words  $x = x_{\pm}^-$  are points of analyticity for

$$\int_0^1 dy (1 - y)^{\epsilon/2} y \left[ \Gamma(1 + \epsilon) (-y^2 + \mu_x^2) \chi^{-1} + \left(2 - \frac{\epsilon}{2}\right) \Gamma(\epsilon) \right]. \quad (128)$$

This fact remains obviously true after *raising* powers of  $\chi$ , operation that brings negative powers of  $\lambda$  in the result and, due to analyticity of the integrand in those points, we can distort the integration contour. One can reach this conclusion also by following an alternative derivation of the result. Starting from Eq.(109) we apply Eq.(114) only once. The integral will be of the following form:

$$S_{33} = \int_0^1 dx \int_0^1 dy \left( \frac{I_1}{\Lambda} + I_0 \right), \quad \Lambda = \lambda(1, \mu_3^2, \mu_x^2). \quad (129)$$

A simple exercise shows that

$$\int_0^1 dy I_1 = 0, \quad \text{for} \quad \mu_x^2 = (1 - \mu_3)^2, \quad (130)$$

so that we can replace

$$I_1(x, y) \rightarrow I^{\text{sub}}(x, y) = I_1(x, y) - I_1(\mu_x = 1 - \mu_3). \quad (131)$$

Just one iteration of the *raising* procedure gives  $I_{0,1}$  continuous, as compared with two iterations that give also continuous first derivatives but, in this way, the whole integrand is well behaved around the zeros of  $\lambda(1, \mu_3^2, \mu_x^2)$ . As for the one-loop, two-point function, once a suitable integral representation is found, the branch point corresponding to normal threshold is not due to poles of the integrand.

We repeat that distortion of the contour is only dictated by the need of achieving numerical convergence and must satisfy one criterion: the new contour cannot cross the cuts of  $\chi^{-\epsilon}$ . Since

at the normal threshold the two branch points approach each other on the real axis, there we can no longer distort the contour and face numerical instabilities. Therefore, the method cannot be applied, as it stands, when we are exactly at threshold and an alternative algorithm will be presented in Section 3.1.5.

Summarizing, we may say that BT method has the advantage of moving poles into branch points and minimal BT method requires a knowledge of the analytical properties of a one-loop sub-diagram of the whole diagram  $G$ , a task much simpler than the one of knowing the whole analytical structure of  $G$ .

After a discussion on the singularities of  $\lambda$  and of the imaginary parts we continue by performing an integration by parts after the first operation of *raising* the powers. This will be achieved, after inserting Eq.(114) into Eq.(109), with the help of the following relations:

$$\int_0^1 dy y^n (1-y)^{\epsilon/2} \frac{\partial}{\partial y} \ln^m \chi(x, y) = -\delta_{n0} \ln \chi(x, 0) - \int_0^1 dy \left[ n y^{n-1} (1-y)^{\epsilon/2} - \frac{\epsilon}{2} y^n (1-y)^{\epsilon/2-1} \right] \ln^m \chi(x, y), \quad (132)$$

followed by a subtraction procedure that takes care of the  $1-y$  terms,

$$\int_0^1 dy y^n (1-y)^{\epsilon/2-1} \ln^m \chi(x, y) = \frac{2}{\epsilon} \ln^m \chi(x, 1) + \int_0^1 dy (1-y)^{\epsilon/2-1} \times \left[ y^n \ln^m \chi(x, y) - \ln^m \chi(x, 1) \right]. \quad (133)$$

The procedure of *raising* the power of  $\chi$  can be repeated. Since

$$\chi(x, y) = y^2 + 2Ky + L, \quad (134)$$

we could use

$$B \chi^{-\epsilon} = \left[ 1 - \frac{1}{2(1-\epsilon)} (y+Y) \frac{\partial}{\partial y} \right] \chi^{1-\epsilon}, \quad (135)$$

but it is better to expand this relation before integrating by parts, thus avoiding the introduction of fictitious poles at  $\epsilon = 0$ . The result that we obtain by expanding in powers of  $\epsilon$  and by subsequently equating coefficients of the same powers in  $\epsilon$  is as follows:

$$\begin{aligned} B \ln \chi &= \chi \ln \chi + \frac{1}{2} (y+Y) \frac{\partial}{\partial y} \left[ \chi (1 - \ln \chi) \right], \\ B \ln^2 \chi &= \chi \ln^2 \chi - (y+Y) \frac{\partial}{\partial y} \left[ \chi \left( 1 - \ln \chi + \frac{1}{2} \ln^2 \chi \right) \right]. \end{aligned} \quad (136)$$

In this way terms as  $\ln \chi$  or  $\ln^2 \chi$  are transformed into  $\chi \ln \chi$  and  $\chi \ln^2 \chi$ . However, some care is needed in the presence of terms containing  $\ln(1-y)$ . In this case we proceed as follows:

$$\int_0^1 dy y^n \ln(1-y) \ln \chi = \int_0^1 dy y^n \ln(1-y) \left( \ln \frac{\chi}{\mu_2^2} + \ln \mu_3^2 \right)$$

$$= -\frac{1}{n+1} \ln \mu_3^2 \sum_{j=1}^{n+1} \frac{1}{j} + \int_0^1 dy y^n \ln(1-y) \ln \frac{\chi}{\mu_3^2}, \quad (137)$$

where use has been made of the relation  $\chi(x, 1) = \mu_3^2$ . In this case the quadratic form in  $y$  to which we apply the algorithm is

$$\frac{y^2}{\mu_3^2} + 2 \frac{K}{\mu_3^2} y + \frac{L}{\mu_3^2}, \quad (138)$$

giving  $B$  and  $Y$  coefficients,

$$B = \frac{\lambda}{\mu_3^2} \quad Y = K. \quad (139)$$

Therefore we will have terms of the following form:

$$\int_0^1 dy y^n \ln(1-y) \frac{\partial}{\partial y} (\chi \ln \chi), \quad (140)$$

which, after integration by parts, become

$$- \int_0^1 dy \chi \ln \frac{\chi}{\mu_3^2} \left[ n y^{n-1} \ln(1-y) + \frac{y^n}{y-1} \right]. \quad (141)$$

In this way we arrive at our final formulas for  $S_{33}$  which is shown explicitly in Appendix C. The other  $S_{3i}$  terms follow through the permutations of Eq.(97).

### 3.1.3 Evaluation of $S_{3p}$

The remaining contribution is  $S_{3p}$ , defined in Eq.(89). Everything proceeds as in Section 3.1.2, in particular the double-pole turns out to be zero and the single-pole is

$$\frac{1}{2} s \left[ \Delta_{UV} - \frac{1}{\epsilon} \right], \quad (142)$$

with  $\Delta_{UV}$  defined in Eq.(106). The complete expression for  $S_{3p}$  is also given in Appendix C. Collecting the various terms we obtain the following expression for  $S_3$ :

$$\begin{aligned} S_{3\text{double-pole}} &= \sum_{i=1}^3 m_i^2 \left( \frac{2}{\epsilon^2} + \Delta_{UV}^2 \right), \\ S_{3\text{single-pole}} &= -2 \sum_{i=1}^3 m_i^2 \frac{\Delta_{UV}}{\epsilon} + \left( \Delta_{UV} - \frac{1}{\epsilon} \right) \left[ \sum_{i=1}^3 m_i^2 \left( 2 \ln \frac{m_i^2}{s} - 3 \right) + \frac{s}{2} \right]. \end{aligned} \quad (143)$$

The finite part will also be given in Appendix C.

### 3.1.4 Integration in the complex plane

The integrand for  $S_3$  is now a smooth function but for inverse powers of  $\lambda$  whose zeros are known and their crossing should be avoided by moving the  $x$ -integration from the interval  $[0, 1]$  to the complex plane. Technically speaking, when we are exactly at the normal threshold, our method is no better than any other numerical method. Away from it, the actual shape of the integration path follows (as discussed in Section 3.0.1) from a careful examination of the imaginary part of the logarithms appearing in the integrand. The following recipe will produce the correct imaginary part for  $S_3$ . If  $(1 - \mu_3)^2 \leq (\mu_1 + \mu_2)^2 \leq (1 + \mu_3)^2$  we compute  $x_{\pm}^+$ , while for  $(1 - \mu_3)^2 \geq (\mu_1 + \mu_2)^2$  we compute both  $x_{\pm}^+$  and  $x_{\pm}^-$ . Next we will have to investigate the branch points of the logarithms. The argument of the logarithms is a quadratic form in  $x$ ,

$$\xi(x, y) = -y \left( y - 1 + \mu_3^2 \right) x^2 + \left[ y \left( y - 1 + \mu_3^2 \right) + (1 - y) \left( \mu_2^2 - \mu_1^2 \right) \right] x + (1 - y) \mu_1^2. \quad (144)$$

If the corresponding discriminant is positive we will have two real roots,  $x_{L,R}$ , otherwise we have a pair of complex conjugated roots. In the latter case we select a contour which starts at  $x = 0$  and bypasses  $x = x_{\pm}^+$  or  $x = x_{\pm}^-$ ,  $x_{\pm}^-$  in the upper half-plane to return to  $x = 1$ . The distorted contour must avoid any crossing of the cuts of the logarithm which will be, in this case, parallel to the imaginary  $x$ -axis.

If the roots are real we must distinguish between two cases. Let us denote the quadratic in  $x$  of Eq.(144) as  $ax^2 + bx + c$ , with  $b^2 \geq 4ac$ . If  $a$  is positive then the cut is between  $x_L$  and  $x_R$ , while for negative  $a$  the cut is  $[-\infty, x_L] \cup [x_R, +\infty]$ . Furthermore, if  $x = \alpha + i\beta$ , the imaginary part of the logarithm is  $\beta(2\alpha a + b)$ . This consideration immediately tells us the sign of the imaginary part when  $x$  approaches the real axis on the cut. This sign is crucial when we distort the contour in the complex plane since, for  $x$  real and on the cut, the  $i\delta$  prescription,

$$\ln(ax^2 + bx + c) \rightarrow \ln(ax^2 + bx + c - i\delta), \quad (145)$$

gives  $-i\pi$  for the imaginary part. To give an example, when the branch points are real and  $a$  is positive, any contour should start at  $x = 0$ , bypass  $x_{\pm}^-$ , return to the real axis from above and for  $\text{Re } x \leq -b/(2a)$ , leave the real axis in the lower half-plane for  $\text{Re } x \geq -b/(2a)$  and bypass  $x_{\pm}^+$  to return to  $x = 1$ . Typical examples are shown in Figs. 9–10.

We now examine the behavior of the integrand close to the normal threshold. Consider Fig. 11 which corresponds to  $s = (m_1 + m_2 + m_3)^2$  for some choice of masses: for  $y$  below some value  $y_0$  we have that  $x_{L,R}$  are complex conjugated and their real part is internal to the interval  $[0, 1]$ . Just below  $y_0$  the two imaginary parts go to infinity and above  $y_0$  the two branch points become real but are external to  $[0, 1]$ . Furthermore, for some value  $y_{\text{th}}$  the two complex roots  $x_{L,R}$  pinch the integration contour at  $x = x_{\pm}^- \equiv x_{\mp}^+$ . Therefore, any distortion of it will inevitably cross the cut, giving the wrong answer. In a word, we cannot distort the contour any longer. Note that there is no crossing of poles implied here, only a serious problem of numerical convergence of the minimal BT approach due to negative powers of  $\lambda(1, \mu_3^2, \mu_x^2)$  which exhibits a double zero at  $x = x_{\pm}^- \equiv x_{\mp}^+$ . For different choices of the internal masses, at threshold, we may have a different behavior of  $x_{L,R}$

but there will always be a  $y_{\text{th}}$  where they are complex conjugated, with their real part approaching  $x = x_- \equiv x_+^-$  and with imaginary parts pinching the real axis.

The situation at pseudo-threshold,  $s = (m_1 + m_2 - m_3)^2$ , is different as one can see from Fig. 12. Below some value  $y_0$  the roots  $x_{L,R}$  are complex conjugated but the absolute value of the imaginary part has a minimum and, therefore no pinch will occur. Above  $y_0$  the roots are real but external to the interval  $[0, 1]$ . Therefore a distortion of the integration contour, to avoid the point  $x = x_-^+ \equiv x_+^+$ , is always possible.

### 3.1.5 The normal threshold for the sunset

The arguments developed in Section 3.1.4 show that we have to use some other algorithm at the normal threshold  $s = (m_1 + m_2 + m_3)^2$ . Actually, for  $S_{3i}$  and  $S_{3p}$  we have a much simpler derivation of the result which, although different from the BT-approach, allows us to *raise* powers. We consider again Eq.(109) and apply directly Eq.(107). After the expansion around  $n = 4$  we have the following integrations by parts:

$$\begin{aligned} \int_0^1 dy y^n \ln(1-y) \partial_y \ln \chi(x, y) &= - \int_0^1 dy \ln \frac{\chi(x, y)}{\chi(x, 1)} \left[ n y^{n-1} \ln(1-y) - \frac{y^n}{1-y} \right], \\ \int_0^1 dy y^n \ln \chi(x, y) \partial_y \ln \chi(x, y) &= \frac{1}{2} \left[ \ln^2 \chi(x, 1) - \delta_{n,0} \ln^2 \chi(x, 0) - n \int_0^1 dy y^{n-1} \ln^2 \chi(x, y) \right], \\ \int_0^1 dy y^n \partial_y \ln \chi(x, y) &= \ln \chi(x, 1) - \delta_{n,0} \ln \chi(x, 0) - n \int_0^1 dy y^{n-1} \ln \chi(x, y). \end{aligned} \quad (146)$$

Using these relations we obtain a very simple expression for the finite part of  $S_{33}$ ,

$$\begin{aligned} S_{33}^{\text{fin}} &= \int_0^1 dx \int_0^1 dy \left[ \ln \xi(x, y) + \left( \frac{\ln \xi(x, y)}{y-1} \right)_+ \right] + \ln \mu_3^2 (\ln \mu_3^2 - 4) + \frac{13}{2} + \frac{1}{2} \zeta(2), \\ S_{3p}^{\text{fin}} &= \int_0^1 dx \int_0^1 dy, y \ln \xi(x, y) + \frac{3}{8}, \end{aligned} \quad (147)$$

where  $\xi = x(1-x)\chi$  and the ‘+’-distribution is defined by Eq.(181) of Appendix C. Therefore, we have reached our goal of expressing the result in terms of a smooth integrand, without obnoxious overall factors that can vanish in certain regions with a consequent numerical instability. The reason why we have not indicated Eq.(147) as the main result of our work is based on the fact that the same result cannot be generalized for other topologies. Indeed, it is essential to have the factor  $\mu_x^2 - y^2$  and, therefore, Eq.(107) can be applied only once. However, we have now a result that can be used for the sunset diagram, without numerical instabilities, also at threshold. Numerical results will be shown in the next sections.

For other topologies we will use the minimal BT-approach everywhere but at the corresponding normal thresholds and will adapt the present algorithm around them. Actually there are cases where the result is again very simple.

– *The  $S_4$  topology:*



The  $S_4$  topology is given by

$$\pi^4 S_4 = \mu^{2\epsilon} \int d^n q_1 d^n q_2 \frac{1}{(q_1^2 + m_1^2) \left( (q_1 - q_2)^2 + m_2^2 \right) (q_2^2 + m_3^2) \left( (q_2 + p)^2 + m_4^2 \right)}. \quad (148)$$

We easily derive the following relation:

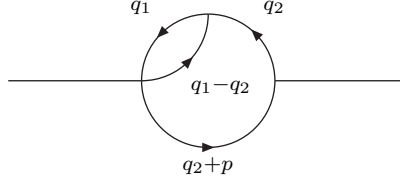


Figure 8: The two-loop diagram  $S_4$ . Arrows indicate the momentum flow.

$$S_4 = (\epsilon - 1) \int_0^1 dx S_{33} (x^2 p^2; m_1, m_2, M_x),$$

$$M_x^2 = -p^2 x^2 + (p^2 + m_4^2 - m_2^2)x + m_3^2, \quad (149)$$

where

$$(\epsilon - 1) S_{33}^{\text{fin}} (x^2 p^2; m_1, m_2, M_x) = - \int_0^1 dy \int_0^1 dz \left[ \ln \xi(y, z) + \left( \frac{\ln \xi(y, z)}{z - 1} \right)_+ \right] + \ln M_x^2 (2 - \ln M_x^2)$$

$$- \frac{7}{2} - \frac{1}{2} \zeta(2), \quad (150)$$

and  $\xi$  is given in Eq.(144), with  $p^2 \rightarrow x^2 p^2$ . For other cases the result is more involved.

– *Other topologies:*

The key observation is that any two-loop diagram can be written as a multi-dimensional integral, over *external* Feynman parameters  $x_{\text{ext}}$ , of a kernel which is nothing but a generalized sunset topology with masses that depend on  $x_{\text{ext}}$ ,

$$D = \prod_{i=1, N} \int_0^1 dx_{\text{ext}}^i (\alpha, m_1 | \gamma, m_2, p | \beta, m_3). \quad (151)$$

Around thresholds, where nothing better will work, we make use of recurrence relations, for instance

$$(\alpha + 1, m_1 | \gamma, m_2, p | \beta, m_3) = -\frac{1}{\alpha} \frac{\partial}{\partial m_1^2} (\alpha, m_1 | \gamma, m_2, p | \beta, m_3), \quad (152)$$

until we reach  $(1, m_1 | 1, m_2, p | 2, m_3)$  where a stable numerical result can be produced. At this point, despite the poor reputation enjoyed by numerical differentiation, we will perform all differentiations with respect to masses numerically. Only at the end the final integration over  $x_{\text{ext}}$  will be executed<sup>1</sup>.

<sup>1</sup>However, a detailed study of two-loop self-energies [57] shows that, in these cases, numerical differentiation can be avoided in favor of alternative realizations of the *raising* procedure

### 3.1.6 Special cases and numerical results

The whole algorithm presented in the previous sections has been translated into a FORM code [60] and the output has been used to create a FORTRAN code<sup>2</sup> that computes  $S_3$ . Some of the results are shown in the following sub-section where they are compared with the analytical results that are available in the literature for some special cases. When some of the masses are zero the result for  $S_3$  simplifies. For  $m_1 = 0$  we obtain

$$S_3(p^2; 0, m_2, m_3) = m_2^2 S_{32}(p^2; 0, m_3, m_2) + m_3^2 S_{33}(p^2; 0, m_2, m_3) + S_{3p}(p^2; 0, m_3, m_2). \quad (153)$$

For  $m_2 = 0$  or  $m_3 = 0$  we use Eq.(153) and the following properties:

$$S_3(p^2; m_1, m_2, m_3) = S_3(p^2; m_2, m_1, m_3) = S_3(p^2; m_3, m_2, m_1). \quad (154)$$

Finally, if two masses are zero we use the appropriate permutation and

$$S_3(p^2; 0, m_2, 0) = m_2^2 S_{32}(p^2; 0, 0, m_2) + S_{3p}(p^2; 0, 0, m_2). \quad (155)$$

For  $m_1 = m_3 = 0$  we have an analytical result [61] (see also ref. [62]). With

$$z = \frac{s}{m^2} + i\delta, \quad \Delta_{UV}(z) = \Delta_{UV} - \ln z, \quad (156)$$

we derive the real and imaginary parts of  $S_3$ :

$$\begin{aligned} \text{Re}S_3(p^2; 0, m, 0) &= m^2 \left[ \frac{2}{\epsilon^2} + \frac{1}{\epsilon} \left( 3 - \frac{1}{2}z - 2\Delta_{UV} + 2 \ln z \right) + \frac{1}{2} \left( z - \frac{1}{z} \right) \ln |z - 1| \right. \\ &\quad \left. + \text{Re Li}_2(z) + 3 + \frac{1}{2}z \Delta_{UV}(z) - \frac{13}{8}z + \Delta_{UV}^2(z) - 3 \Delta_{UV}(z) + \frac{3}{2} \zeta(2) \right], \\ \text{Im}S_3(p^2; 0, m, 0) &= m^2 \text{Im} \left[ \frac{1}{2} \left( z - \frac{1}{z} \right) \ln(1 - z) + \text{Li}_2(z) \right]. \end{aligned} \quad (157)$$

For the numerical evaluation we have used the NAG [63] Fortran library subroutine D01EAF that integrates a vector of similar functions (e.g. real and imaginary parts of the scalar diagram) over the same multi-dimensional hyper-rectangular region. In certain regions, e.g. around thresholds, one obtains moderately accurate results and for these cases we switch to the routine D01GDF, a multi-dimensional quadrature for general product regions, using number-theoretic methods.

A detailed comparison is shown between the numerical approach based on the minimal BT-algorithm and the analytical result of Eq.(157) in Tab. 3. There we use  $m_1 = m_3 = 0$ ,  $m_2 = 1.765$  GeV and moreover we select  $\epsilon = 1$  and  $\mu = 1$  GeV. Note that there is no loss of numerical precision near, but not too near, the normal thresholds. The requested precision for the integration routine is of a relative error of  $10^{-5}$ . Comparison with the analytical result shows that the returned numerical error is overestimated with a very good agreement over a wide range of values for  $\sqrt{s}$ .

$\sqrt{s}$ [GeV]	Re $S_3$	Im $S_3$	$\sqrt{s}$ [GeV]	Re $S_3$	Im $S_3$
0.5	15.055283(146)	0	4	18.534988(176)	-8.249166(53)
	15.055293	0		18.534996	-8.249165
1	15.440106(120)	0	6	31.015475(323)	-32.328029(149)
	15.440114	0		31.015477	-32.328028
1.5	15.996235(151)	0	8	59.575707(705)	-70.918158(379)
	15.996239	0		59.575722	-70.918157
1.7	16.228067(165)	0	10	106.89072(123)	-123.22756(69)
	16.228068	0		106.89073	-123.22756
1.8	16.333331(172)	-0.000196(4)	50	6572.7884(387)	-3862.1006(247)
	16.333332	-0.000196		6572.7846	-3862.1002
2	16.491314(184)	-0.028545(7)	100	33332.656(159)	-15629.648(102)
	16.491316	-0.028545		33332.642	-15629.648

Table 3: The sunset topology  $S_3$  for  $m_1 = m_3 = 0$  and  $m_2 = 1.756$  GeV as a function of  $\sqrt{s}$ . First entry is the minimal BT-approach, second entry is the analytical result of Eq.(157). The UV-pole is  $\epsilon = 1$  and the unit of mass is  $\mu = 1$  GeV.

To investigate in more detail the situation around  $s = m_2^2$  we have produced Tab. 4. From it we see that by approaching  $\sqrt{s} = m_2$  up to  $1 - \sqrt{s}/m_2 = 3.4 \times 10^{-3}$  we register an increasing numerical error on the real part, although the relative deviation from the analytical result is better than  $10^{-4}$  signalling, once more, the conservative estimate of the numerical error. For the imaginary part, immediately after threshold, the numerical convergence is poor in a situation where the result is very small. At  $1.4 \times 10^{-2}$  away from threshold, however, we register again an excellent agreement.

As explained in Section 3.1.5, however, around the normal threshold we can produce an accurate result by using Eq.(147). Results for a scan around and at threshold are shown in Tab. 5. Another comparison concerns the imaginary part of  $S_3$  which is finite in four dimensions and can be derived analytically by reduction to Legendre form of elliptic integrals. The complete expression is given in ref. [61] and, here, we only give a detailed comparison. The result is shown in Tab. 6 where we compare two different methods of numerical integration. We find better and better agreement

<sup>2</sup>FORTTRAN may be archaic but never leaves you in solitude.

$\sqrt{s}$ [GeV]	Re $S_3$	Im $S_3$	$\sqrt{s}$ [GeV]	Re $S_3$	Im $S_3$
1.732	16.26311(2) 16.26311	0 0	1.762	16.29475(1238) 16.29495	* $-0.51 \times 10^{-6}$
1.740	16.27171(10) 16.27171	0 0	1.772	16.30528(22) 16.30529	$-0.9(5) \times 10^{-5}$ $-0.96 \times 10^{-5}$
1.750	16.28075(13643) 16.28235	0 0	1.780	16.31344(4) 16.31344	$-0.324(8) \times 10^{-4}$ $-0.323 \times 10^{-4}$

Table 4: A scan of the sunset,  $S_3$ , topology for  $m_1 = m_3 = 0$  and  $m_2 = 1.756$  GeV around the normal threshold  $s = (m_1 + m_2 + m_3)^2$ . First entry is the minimal BT-approach, second entry is the analytical result of Eq.(157). A \* indicates poor numerical convergence in the numerical evaluation. Note, however, that this table is only for illustration and, in this region, one should always use Eq.(147) (see Tab. 5). The UV-pole is  $\epsilon = 1$  and the unit of mass is  $\mu = 1$  GeV.

away from thresholds with a numerical error that, in general, overestimate the difference with the analytical result. Indeed, near threshold, we have a relative difference of 0.017%(0.005%) with a returned numerical error of 0.79%(0.74%).

Finally, following the suggestion of ref. [61], we introduce a special combination:

$$\begin{aligned}
S_c = & S_3(p^2; m_1, m_2, m_3) - S_3(p^2; m_1, 0, m_3) \\
& - S_3(p^2; 0, m_2, m_3) - S_3(p^2; 0, 0, m_3),
\end{aligned} \tag{158}$$

where infinite parts cancel. For small  $|p^2|$ , essentially for  $|p^2| < m_3^2$ , the combination  $S_c$  is known in the form of a multiple series in the variables

$$z_1 = \frac{m_1^2}{m_3^2}, \quad z_2 = \frac{m_2^2}{m_3^2}, \quad z_3 = \frac{s}{m_3^2}, \tag{159}$$

with  $s = -p^2$ . The comparison is shown in Tab. 7 for  $p^2$  space-like or time-like, showing excellent agreement with the analytical result derived from the expansion of a Lauricella function.

### 3.2 Tensor integrals

Tensor integrals of the type

$$(\mu_1 \dots \mu_i \mid \nu_1 \dots \nu_j \mid 1, m_1 \mid 1, m_2, p \mid 1, m_3), \tag{160}$$

$\sqrt{s}$ [GeV]	Re $S_3$	Im $S_3$	$\sqrt{s}$ [GeV]	Re $S_3$	Im $S_3$
1.732	16.2631072(1) 16.2631072	0 0	1.762	16.2949492(1) 16.2949492	$-0.512620701(1) \times 10^{-6}$ $-0.512620700 \times 10^{-6}$
1.740	16.2717059(1) 16.2717059	0 0	1.772	16.3052845(1) 16.3052845	$-0.963868786(1) \times 10^{-5}$ $-0.963868786 \times 10^{-5}$
1.750	16.2823493(1) 16.2823493	0 0	1.780	16.3134359(1) 16.3134359	$-0.323117581(1) \times 10^{-4}$ $-0.323117581 \times 10^{-4}$
threshold	16.2886745(1) 16.2886745	0 0			

Table 5: The same as in Tab. 4 but using Eq.(147). Integration is performed with the NAG subroutine D01GDF.

are usually decomposed into scalar integrals. For a general discussion we refer to the work of ref. [59] where the following functions are introduced:

$$(\epsilon-1)\mathcal{P}_{112}^{ij} = \left( \underbrace{p \dots p}_i \mid \underbrace{p \dots p}_j \mid 1, m_1 \mid 1, m_2, p \mid 2, m_3 \right) = (i, p \mid j, p \mid 1, m_1 \mid 1, m_2, p \mid 2, m_3), \quad (161)$$

where  $i + j \leq 3$ . It is easily shown that these integrals admit the following representation:

$$\mathcal{P}_{112}^{ij} = \left( \frac{\mu^2}{\pi} \right)^\epsilon \frac{\Gamma(\epsilon)}{\epsilon-1} \sum_{n=-1}^{+1} \int_0^1 dx \int_0^1 dy [x(1-x)]^{-\epsilon/2} y(1-y)^{\epsilon/2} Q_n^{ij}(x, y, \epsilon) U^{n-\epsilon}(x, y), \quad (162)$$

where  $U$  is given in Eq.(102). Therefore, to each of these functions we apply the minimal BT-algorithm and derive expressions similar to those obtained for  $S_{33} = \mathcal{P}_{112}^{00}$ . The polynomials  $Q$  are as follows:

$$Q_{-1}^{00} = 2(m_x^2 + y^2 p^2), \quad Q_0^{00} = \frac{4}{\epsilon} - 1, \quad Q_1^{00} = 0,$$

$$Q_{-1}^{10} = -2xyp^2(m_x^2 + y^2 p^2), \quad Q_0^{10} = xyp^2\left(1 - \frac{6}{\epsilon}\right), \quad Q_1^{10} = 0,$$

$\sqrt{s}$ [GeV]	Im $S_3$	Im $S_3$ (analytical)	$\sqrt{s}$ [GeV]	Im $S_3$	Im $S_3$ (analytical)
255	-32.038(253) -32.046(237)	-32.044	295	-6464.878(259) -6464.404(517)	-6464.877
265	-616.707(256) -617.210(201)	-616.717	300	-7995.983(258) -7995.226(164)	-7995.056
275	-1906.548(257) -1906.891(327)	-1906.560	400	-66930.101(220) -66930.175(418)	-66930.105
285	-3866.374(258) -3866.388(421)	-3866.289	500	-171686.26(17) -171684.32(67)	-171686.23

Table 6: Im  $S_3$ , the imaginary part of the sunset topology, for  $m_1 = m_3 = 80.448$  GeV and  $m_2 = 91.1875$  GeV as a function of  $\sqrt{s}$ . First entry is the minimal BT-approach, first row integrated with D01EAF, second row with D01GDF and Eq.(147); second entry is the analytical result of ref. [61].

$$Q_{-1}^{20} = 2x^2y^2p^4(m_x^2 + y^2p^2) + 2x(1-x)\frac{p^2}{\epsilon-2}(m_x^2 + y^2p^2)^2,$$

$$Q_0^{20} = x^2p^2\left(\frac{m_x^2 + 9y^2p^2}{\epsilon} - y^2p^2\right) + 2x(1-x)p^2\left(\frac{-2m_x^2 - 3y^2p^2}{\epsilon} + \frac{m_x^2 + 2y^2p^2}{\epsilon-2}\right),$$

$$Q_1^{20} = x^2p^2\left(-\frac{3}{\epsilon} + \frac{5}{2}\frac{1}{\epsilon-1}\right) + x(1-x)p^2\left(\frac{6}{\epsilon} + \frac{2}{\epsilon-2} - \frac{15}{2}\frac{1}{\epsilon-1}\right),$$

$$Q_{-1}^{30} = -2x^3y^3p^6(m_x^2 + y^2p^2) - 6x^2(1-x)y\frac{p^4}{\epsilon-2}(m_x^2 + y^2p^2)^2,$$

$$Q_0^{30} = x^3yp^4\left(\frac{3m_x^2 + 13y^2p^2}{\epsilon} + y^2p^2\right) + x^2(1-x)yp^4\left(6\frac{3m_x^2 + 4y^2p^2}{\epsilon} - 6\frac{2m_x^2 + 3y^2p^2}{\epsilon-2}\right),$$

$$Q_1^{30} = x^3yp^4\left[\frac{9}{\epsilon} - \frac{15}{2}\frac{1}{\epsilon-1} + \frac{3}{\epsilon+4}\left(\frac{4}{\epsilon} - \frac{5}{\epsilon-1}\right)\right] + x^2(1-x)yp^4\left(-3\frac{36}{\epsilon} - \frac{18}{\epsilon-2} + \frac{105}{2}\frac{1}{\epsilon-1}\right),$$

$$Q_{-1}^{01} = 2(1-y)p^2(m_x^2 + y^2p^2), \quad Q_0^{01} = p^2\left(2\frac{2-3y}{\epsilon} - 1 + y\right), \quad Q_1^{01} = 0,$$

$s$ [GeV <sup>2</sup> ]	Re $S_c$	Re $S_c$ (multiple series)	$10^5 \times$ Dev.
- 1	-70.686011	-70.685698	0.44
+ 1	-70.680106	-70.679831	0.39
- 25	-70.756299	-70.756203	0.14
+ 25	-70.609231	-70.609519	0.41
- 81	-70.921481	-70.921413	0.10
+ 81	-70.446044	-70.446147	0.15

Table 7: Re  $S_c$  (see Eq.(158) for the definition) for  $m_1 = 10$  GeV,  $m_2 = 20$  GeV and  $m_3 = 100$  GeV as a function of  $p^2$ . First entry is the minimal BT-approach, second entry is the analytical result of ref. [61]. The UV-pole is  $\epsilon = 1$  and the unit of mass is  $\mu = 1$  GeV.

$$Q_{-1}^{02} = 2p^4(1-y)^2(m_x^2 + y^2p^2),$$

$$Q_0^{02} = p^2 \left[ \frac{m_x^2 + p^2(4 - 12y + 9y^2)}{\epsilon} - p^2(1-y)^2 \right],$$

$$Q_1^{02} = p^2 \left( -\frac{3}{\epsilon} + \frac{5}{2} \frac{1}{\epsilon - 1} \right),$$

$$Q_{-1}^{03} = 2p^6(1-y)^3(m_x^2 + y^2p^2)$$

$$Q_0^{03} = p^4 \left[ \frac{3(1-y)m_x^2 + (4 - 18y + 27y^2 - 13y^3)p^2}{\epsilon} - (1-y)^2p^2 \right],$$

$$Q_1^{03} = p^4 \left[ -9 \frac{1-y}{\epsilon} + \frac{15}{2} \frac{1-y}{\epsilon - 1} + \frac{3}{\epsilon + 4} \left( \frac{4}{\epsilon} - \frac{5}{\epsilon - 1} \right) \right],$$

$$Q_{-1}^{11} = -2xy(1-y)p^4(m_x^2 + y^2p^2),$$

$$Q_0^{11} = xp^2 \left[ 3 \frac{2m_x^2 - 2yp^2 + 3y^2p^2}{\epsilon} + y(1-y)p^2 \right],$$

$$Q_1^{11} = xp^2 \left( -\frac{3}{\epsilon} + \frac{5}{2} \frac{1}{\epsilon - 1} \right),$$

$$\begin{aligned}
Q_{-1}^{21} &= 2x^2y^2(1-y)p^6(m_x^2 + y^2p^2) + 2x(1-x)(1-y)\frac{(m_x^2 + y^2p^2)^2}{\epsilon - 2}, \\
Q_0^{21} &= x^2p^4\left[\frac{(1-3y)m_x^2 + y^2p^2(9-13y)}{\epsilon} - y^2(1-y)p^2\right] \\
&\quad + x(1-x)\left[\frac{2(3y-2)m_x^2 + 2y^2p^2(4y-3)}{\epsilon} + \frac{2(1-2y)m_x^2 + 2y^2p^2(2-3y)}{\epsilon - 2}\right], \\
Q_1^{21} &= x^2p^4\left[\frac{3(3y-1)}{\epsilon} + \frac{5}{2}\frac{1-3y}{\epsilon-1} + 3\frac{1}{\epsilon+4}\left(\frac{4y}{\epsilon} - \frac{5y}{\epsilon-1}\right)\right] \\
&\quad + x(1-x)(1-3y)\left[6\frac{1}{\epsilon} + \frac{2}{\epsilon-2} - \frac{15}{2}\frac{1}{\epsilon-1}\right], \\
Q_{-1}^{12} &= -2xy(1-y)^2p^6(m_x^2 + y^2p^2), \\
Q_0^{12} &= xp^4\left[\frac{(2-3y)m_x^2 - y(6-18y+13y^2)p^2}{\epsilon} + y(1-y)^2p^2\right], \\
Q_1^{12} &= xp^4\left[\frac{-3(3y-2)}{\epsilon} + 5\left(1-\frac{3}{2}\right)\frac{1}{\epsilon-1} + \frac{3}{\epsilon+4}\left(\frac{4}{\epsilon} - \frac{5}{\epsilon-1}\right)\right]. \tag{163}
\end{aligned}$$

In our approach we avoid using derivatives with respect to the external parameters since the poor reputation enjoyed by numerical differentiation leads to search for techniques which avoid the explicit use of it. Conversely our numerical integration is usually performed with the help of the NAG [63] Fortran library subroutine D01EAF that computes approximations to the integrals of a vector of similar functions over the same multi-dimensional hyper-rectangular region. Therefore all relevant integrals, connected to the  $S_3$  topology (any topology), are computed in one stroke without any noticeable loss of CPU time with respect to computing the scalar integral alone. Therefore we introduce additional tensor integrals of the following form:

$$\begin{aligned}
(\epsilon - 1) \mathcal{P}_{112}^{1|j} &= (\mu\mu | \underbrace{p \dots p}_j | 1, m_1 | 1, m_2, p | 2, m_3), \\
(\epsilon - 1) \mathcal{P}_{112}^{2|i} &= (\underbrace{p \dots p}_i | \mu\mu | 1, m_1 | 1, m_2, p | 2, m_3), \tag{164}
\end{aligned}$$

where  $i, j = 0, 1$ . They also can be cast into the form

$$\mathcal{P}_{112}^{1,2|i} = \left(\frac{\mu^2}{\pi}\right)^\epsilon \frac{\Gamma(\epsilon)}{\epsilon-1} \sum_{n=-1}^{+1} \int_0^1 dx \int_0^1 dy [x(1-x)]^{-\epsilon/2} y(1-y)^{\epsilon/2} Q_n^{1,2|i}(x, y, \epsilon) U^{n-\epsilon}(x, y), \tag{165}$$

with corresponding polynomials that will not be presented in this paper. Other integrals can be easily derived by applying  $(\alpha\beta\gamma)$  partial integration, for instance

$$\begin{aligned}
(i, p | j, p | 1, m_1 | 1, m_2, p | 1, m_3) &= \frac{1}{\epsilon - 1 - (i+j)/2} \left[ \right. \\
m_1^2 (i, p | j, p | 2, m_1 | 1, m_2, p | 1, m_3) &+ (p^2 + m_2^2) (i, p | j, p | 1, m_1 | 2, m_2, p | 1, m_3) + \left. \right]
\end{aligned}$$



$$m_3^2 \left( i, p \mid j, p \mid 1, m_1 \mid 1, m_2, p \mid 2, m_3 \right) + \left( i + 1, p \mid j, p \mid 1, m_1 \mid 2, m_2, p \mid 1, m_3 \right) + \left( i, p \mid j + 1, p \mid 1, m_1 \mid 2, m_2, p \mid 1, m_3 \right)]. \quad (166)$$

The tensor integrals are easily computed and, once the method will be extended to cover all two-loop topologies, one may start organizing a realistic calculation. However, in any realistic calculation, the general strategy will be substantially different from the one usually adopted in one-loop exercises. It will be more convenient to write a Form code for any two-loop diagram  $G$ , or set of diagrams  $\sum_j G_j$ , that produces one expression of the form

$$\int_S dx \sum_{ij} Q_{ij}(x) V_{G_j}^{-\mu_j}(x), \quad (167)$$

and to apply the method directly to this integral instead of applying first the tensor decomposition and then to compute, separately, the various  $ij$  components of the total result. In a way one loses some attractive feature of the analytical one-loop approach, where few universal building blocks are needed and everything is algebraically reduced to those blocks. But, again, this is a typical example of a procedure motivated by our ability to derive analytical results. The perspective, here, is radically different, see ref. [50] for an epistemological discussion.

## 4 Conclusions

In this paper we have considered the Bernstein-Tkachov algorithm, proposed in [50], which proves of some use in dealing with fast and accurate numerical evaluation of arbitrary multi-loop Feynman diagrams.

As a prelude, we have applied the BT algorithm to one-loop diagrams with an arbitrary number of external legs, where reliable analytical results have been known for a long time, to show the feasibility of a project based on this new strategy and to discuss, with simple examples, the infrared divergent cases and the new approach that one will have to adopt in dealing with reduction of tensor integrals.

After this brief excursus in the one-loop world we have considered the application of the algorithm to genuine multi-loop diagrams. Vacuum and tadpole diagrams and two-loop diagrams at zero external momentum allow for a full implementation of the method but, in general, we have not succeeded in deriving the basic ingredient, i.e. the polynomial  $P$  of Eq.(1)<sup>3</sup>. Therefore, we have introduced a variant of the original proposal, a minimal BT-approach, which can be described as the convolution of the Ghinculov and Yao techniques, especially the use of complex Feynman parameters, with the basic BT-algorithm of *raising* powers in Feynman integrands. The main idea is related to the simple observation that we know how to apply the BT-iterative procedure

---

<sup>3</sup>To the best of our knowledge no example is known in the literature beyond the one-loop case of [50]. Working with some unrealistic case S. Uccirati has shown how to deal with cubic polynomials in two variables where, however, the coefficient  $B$  of Eq.(1) contains approximately  $3 \times 10^4$  terms.

of *raising* powers for an arbitrary one-loop diagram. Therefore, given any two-loop diagram  $G$  we minimally apply BT functional relation to the one-loop sub-diagram  $L \in G$  which has the largest number of internal lines. In this way the integrand can be made smooth, a part from the factor  $B$  of Eq.(1) which is now a polynomial in  $x_s$ , the set of Feynman parameters needed for the complementary one-loop sub-diagram  $S \in G$  with the smallest number of internal lines. Since the BT procedure does not introduce singularities through  $B$ , a part from the singularities of  $G$  itself in the external parameter space, before performing the  $x_s$ -integration we move the contour into the complex hyper-plane, thus avoiding the crossing of apparent singularities. This is the procedure introduced in [59].

The minimal BT-approach has been applied to the sunset two-loop diagram and numerical results are shown, comparing them with the relevant literature. Whenever available, published results for the sunset show excellent agreement with our method which is fast and accurate in all regions, time-like or space-like external momentum, around normal thresholds and pseudo-thresholds.

However, when we are close enough to the normal threshold the integration contour cannot be distorted and numerical instabilities appear.

A preliminar analysis of other two-loop diagrams leads us to formulate the conjecture that these numerical instabilities are always connected with the leading Landau singularity of the original diagram.

In these regions we have found more convenient to apply another algorithm for *raising* powers which gives a very simple result, although with discontinuous imaginary part of the integrand. Therefore, very accurate predictions can be made also at the normal threshold. The extension of this variant of the *raising* procedure to other two-loop topologies may require the introduction of numerical differentiation with respect to masses which is, in general, an unsatisfactory branch of numerical analysis. However, close to normal threshold, this alternative procedure represents the safest way for a numerical evaluation of diagrams, unless one want to adopt specific expansions that can be found in the literature. A preliminar analysis [57] has shown that, for two-point functions and one iteration, a transformation of the Feynman parameters can always be found that produces a coefficient  $B$   $x_s$ -independent. This  $B$  will vanish at some non-leading Landau singularity of the diagram where additional analytical work is needed before starting the numerical evaluation.

Work is in progress to extend the method to all two-loop, two-(three-)point topologies and we plan to extend it to all two-loop diagrams with the evident goal of performing a complete two-loop analysis of the standard model predictions, in particular of quantities like  $\sin^2 \theta_{\text{eff}}^l$  at the level of  $1 \times 10^{-6}$  theoretical precision.

## Acknowledgments

I would like to express my gratitude to Fyodor Tkachov for several discussions on the general idea of evaluating multi-loop Feynman diagrams numerically. I sincerely thank Dmitri Bardin for

being stronger than my stubbornness and for finally succeeding in drawing my full attention to the work of Fyodor Tkachov during several walks in Dubna, in Summer 2000. The contribution of Sandro Uccirati for evaluating pentagon and hexagon one-loop integrals is also acknowledged.

## 5 Appendix A

In this Appendix we give details about the analytical derivation of double and single UV poles for  $S_{33}$ , defined in Eq.(89). First we use the Laurent expansion of  $\Gamma(z)$  around  $z = 0$ ,

$$\Gamma(z) = \frac{1}{z} - \gamma + \frac{1}{2} [\gamma^2 + \zeta(2)]x - \frac{1}{6} [\gamma^3 + 3\zeta(2) + 2\zeta(3)]z^2 + \mathcal{O}(z^3). \quad (168)$$

Next we introduce

$$\chi(x, y) = \frac{\xi(x, y)}{x(1-x)}, \quad (169)$$

and expand in  $\epsilon$  the various terms as follows:

$$\begin{aligned} (1-y)^{\epsilon/2} &= 1 + \frac{\epsilon}{2} \ln(1-y) + \frac{\epsilon^2}{8} \ln^2(1-y) + \mathcal{O}(\epsilon^3), \\ [x(1-x)]^{l+\epsilon/2} &= [x(1-x)]^l \left[ 1 + \frac{\epsilon}{2} \ln(x-x^2) + \frac{\epsilon^2}{8} \ln^2(x-x^2) + \mathcal{O}(\epsilon^3) \right], \\ \xi^{-1-\epsilon} &= \xi^{-1} \left[ 1 - \epsilon \ln \xi + \frac{\epsilon^2}{2} \ln^2 \xi + \mathcal{O}(\epsilon^3) \right]. \end{aligned} \quad (170)$$

Some of the integrals can be performed directly by using the following relations:

$$\begin{aligned} \int_0^1 dy y^n \ln^2(1-y) &= \int_0^1 dy (1-y)^2 \ln^2 y, \\ \int_0^1 dy y^n \ln^2 y &= \frac{2}{(n+1)^3}, \\ \int_0^1 dy y^n \ln(1-y) &= -\frac{1}{n+1} \sum_{j=1}^{n+1} \frac{1}{j}, \\ \int_0^1 dy y^n &= \frac{1}{n+1}, \\ \int_0^1 dx x^n \ln x \ln(1-x) &= \frac{1}{n+1} \sum_{j=1}^{n+1} \frac{1}{j} \left( \frac{1}{n+1} + \frac{1}{j} \right) - \frac{\zeta(2)}{n+1}. \end{aligned} \quad (171)$$

In this way we arrive at the following expression for  $S_{33}$ :

$$\begin{aligned} S_{33} &= \frac{2}{\epsilon^2} - \frac{2}{\epsilon} \left( 1 + \gamma + \ln \pi + \ln \frac{s}{\mu^2} \right) + (\gamma + \ln \pi)^2 \\ &+ \ln \frac{s}{\mu^2} \left( 2 + 2\gamma + \ln \frac{s}{\mu^2} \right) + 2 \ln \pi \left( 1 + \ln \frac{s}{\mu^2} \right) + 2\gamma \\ &+ \int_0^1 dx \int_0^x dy \xi^{-1} \left( \frac{2}{\epsilon} - \gamma - \ln \pi - \ln \frac{s}{\mu^2} \right) [-xy^3(1-x) + yM_x^2] \end{aligned}$$

$$\begin{aligned}
& + \int_0^1 dx \int_0^x dy \xi^{-1} \left[ 2 + \ln(1-y) + \ln(x-x^2) - 2 \ln \xi \right] \left[ -xy^3(1-x) + yM_x^2 \right] \\
& - 4 \int_0^1 dx \int_0^x dy y \ln \xi \left( \frac{1}{\epsilon} - \gamma - \ln \pi - \ln \frac{s}{\mu^2} \right) \\
& + 2 \int_0^1 dx \int_0^x dy y \left[ \ln^2 \xi - \ln(1-y) - \ln(x-x^2) - \frac{3}{2} \ln \xi \right] \\
& + \frac{13}{4} + \frac{\zeta(2)}{2}.
\end{aligned} \tag{172}$$

here we have introduced

$$M_x^2 = (1-x)\mu_1^2 + x\mu_2^2 = x(1-x)\mu_x^2. \tag{173}$$

next we restore  $\xi = x(1-x)\chi$  and make use of the relation Eq.(107). After integration by parts, i.e.

$$\int_0^1 dy \frac{y^n}{\chi} \frac{\partial}{\partial y} \chi = \ln \mu_3^2 - n \int_0^1 dy y^{n-1} \ln \chi, \tag{174}$$

the final result, Eqs.(106)–(108), follows.

## 6 Appendix B

In this appendix we consider the case  $p^2 = -t$ , with  $t < 0$ . Since in this case

$$U(x, y) = -y(1-y)t + ym_3^2 + (1-y)m_x^2, \tag{175}$$

the quadratic form  $\chi$ , for  $t$ -channel diagrams is redefined as

$$U = -t\chi, \quad \chi = y(1-y) + y\mu_3^2 + (1-y)\mu_x^2, \tag{176}$$

with  $\mu^2 = -m^2/t > 0$ . Furthermore, when *raising* the power  $\mu$  in  $\chi^\mu$  for the  $t$ -channel case, we have to change coefficients accordingly:

$$H = -1, \quad K = \frac{1}{2} \left( 1 + \mu_3^2 - \mu_x^2 \right), \quad L = \mu_x^2, \tag{177}$$

which gives

$$B = \frac{1}{4} \lambda \left( 1, -\mu_3^2, -\mu_x^2 \right), \quad Y = -\frac{1}{2} \left( 1 + \mu_3^2 - \mu_x^2 \right), \tag{178}$$

and one should replace

$$\ln \frac{s}{\mu^2} \rightarrow \ln \frac{-t}{\mu^2} \tag{179}$$

in the pole terms.

## 7 Appendix C

In this Appendix we give the explicit integrand for  $S_{33}$ , the other  $S_{3i}$  terms following through the permutations of Eq.(97). First we introduce auxiliary variables

$$\begin{aligned} X &= x(1-x), & A &= X(1-\mu_3^2) + B, \\ B &= X\mu_x^2, & \xi(x,y) &= X\chi(x,y). \end{aligned} \quad (180)$$

The ‘+’-distribution is defined, as usual, by its action on a generic test function  $g(x)$ :

$$\int_0^1 dx g(x) f_+(x) = \int_0^1 dx [g(x) - g(1)] f(x). \quad (181)$$

We also use the notations

$$\ln_+ \xi(x,y) = \ln \xi(x,y) - \ln \xi(x,1), \quad L_x = \ln X, \quad L_y = \ln(1-y). \quad (182)$$

Then we derive the following expressions:

$$S_{33} = S_{33}^{\text{dp}} + S_{33}^{\text{sp}} + S_{33}^{\text{fin}}, \quad S_{33}^{\text{fin}} = \frac{1}{\Lambda} \left[ \frac{I_2}{\Lambda} + I_1 \right] + I_0, \quad \Lambda = X^2 \lambda(1, \mu_3^2, \mu_x^2). \quad (183)$$

Double and single pole parts are defined in Eq.(106) and in Eq.(108) respectively. For the UV finite part we split the final result according to the dimension of the integrals over Feynman parameters,

$$\begin{aligned} I_2 &= \int_0^1 dx \int_0^1 dy I_{22} + \int_0^1 dx I_{21} \\ I_1 &= \int_0^1 dx \int_0^1 dy I_{12} + \int_0^1 dx I_{11} \\ I_0 &= \int_0^1 dx I_{01} + I_{00} \end{aligned} \quad (184)$$

The result is as follows:

$$\begin{aligned} I_{22} &= \xi(x,y) X \left[ 32AB - 48A^2y + 128BXy - \xi(x,y) (42A + 96Xy) \right] L_y \ln_+ \xi(x,y) \\ &+ \xi(x,y) X \left\{ -32AB - 8AX(1-y) + A^2(1+90y) \right. \\ &+ X \left[ -296yB - 32B + X(12+16y) \right] + \xi(x,y) \left[ 64A + X(20+248y) \right] \left. \right\} L_x \\ &+ \xi(x,y) X \left[ 32AB - 48A^2y + 128BXy - \xi(x,y) (42A + 96Xy) \right] \ln \xi(x,y) L_x \\ &+ \xi(x,y) X \left\{ 32AB + 8AX(1-y) - A^2(1+90y) + X \left[ 296yB + 32B - X(12+16y) \right] \right. \\ &- \xi(x,y) \left[ 64A + X(20+248y) \right] \left. \right\} \ln \xi(x,y) \\ &+ \xi(x,y) X \left[ -32AB + 48A^2y - 128BXy + \xi(x,y) (42A + 96Xy) \right] \ln^2 \xi(x,y) \end{aligned}$$

$$\begin{aligned}
& +\xi(x, y) \left( -6ABX + 14AX^2 - 3A^2X + A^2B + 8BX^2 - 16X^2 \right) \left( \frac{\ln \xi(x, y)}{y-1} \right)_+ \\
& +\xi(x, y) X \left\{ -4AB + AX(14 - 2y) - A^2(3 + 5y) + 24BX(y + 1) - 16(y + 1)X^2 \right. \\
& \left. -\xi(x, y) \left[ 2A + 16X(1 + y) \right] \right\} \ln_+ \xi(x, y)
\end{aligned}$$

$$\begin{aligned}
I_{21} = & -\frac{106}{9}ABX^2 + \frac{1658}{75}AX^3 + 11A^2BX - \frac{193}{12}A^2X^2 \\
& +4A_x^3X - 4A_x^3B + \frac{13}{3}BX^3 - \frac{158}{15}X^4 \\
& +X \left[ A \left( -20B^2 + \frac{62}{3}BX + \frac{586}{5}X^2 \right) + A^2(9B - 72X) \right. \\
& \left. +A^3(14X - 4B) + X \left( 24B^2 - 44BX - \frac{176}{3}X^2 \right) \right] L_x \\
& +AX \left( -2B^2 + 2BX - AB + 5AB^2 \right) \ln \xi(x, 0) + A^2B^2 \ln \xi(x, 0)L_x \\
& + \left[ A \left( 22XB^2 - 16X^2B - 126X^3 \right) + A^2 \left( -12XB + 77X^2 - 5B^2 \right) \right. \\
& \left. +A_x^3 \left( -15X + 5B \right) - 24B^2X^2 + 40BX^3 + 64X^4 \right] \ln \xi(x, 1) \\
& + \left[ 6AB^2X - 30AX^3 - 4A^2BX + 17A^2X^2 - A^2B^2 \right. \\
& \left. - 3A_x^3X + A_x^3B - 8B^2X^2 + 8BX^3 + 16X^4 \right] \ln \xi(x, 1)L_x - A^2B^2 \ln^2 \xi(x, 0) \\
& +AX \left[ -6AB^2X + 30AX^3 + 4A^2BX - 17A^2X^2 + A^2B^2 \right. \\
& \left. + 3A_x^3X - A_x^3B + 8B^2X^2 - 8BX^3 - 16X^4 \right] \ln^2 \xi(x, 1)
\end{aligned}$$

$$\begin{aligned}
I_{12} = & \xi(x, y) \left( -2A + 16Xy \right) L_y \ln_+ \xi(x, y) + \xi(x, y) \left( 7A - 40Xy \right) L_x \\
& +\xi(x, y) \left( -2A + 16Xy \right) \ln \xi(x, y)L_x + \xi(x, y) \left( -7A + 40Xy \right) \ln \xi(x, y) \\
& +\xi(x, y) \left( 2A - 16Xy \right) \ln^2 \xi(x, y) + \left( -AX + AB - 2BX + 2X^2 \right) \left( \frac{\ln \xi(x, y)}{y-1} \right)_+ \\
& +\xi(x, y) \left( -2A + 4X \right) \left( \frac{\ln \xi(x, y)}{y-1} \right)_+ + \xi(x, y) \left[ -2A + 4X(1 + y) \right] \ln_+ \xi(x, y)
\end{aligned}$$

$$\begin{aligned}
I_{11} = & AX \left( -\frac{40}{9}AX + 2A^2 - BX + \frac{11}{4}X^2 \right) \\
& +AX \left( -\frac{133}{6}AX - 4AB + 6A^2 + 9BX + \frac{115}{6}X^2 \right) L_x \\
& +AX \left( \frac{149}{6}AX + 4AB - 7A^2 - 7BX - \frac{133}{6}X^2 \right) \ln \xi(x, 1)
\end{aligned}$$

$$\begin{aligned}
& +A \left( 7AX + AB - 2A^2 - 2BX - 6X^2 \right) \ln \xi(x, 1) L_x \\
& +AX \left( -7AX - AB + 2A^2 + 2BX + 6X^2 \right) \ln^2 \xi(x, 1)
\end{aligned}$$

$$I_{01} = -\frac{3}{2} \left[ L_x + \ln \xi(x, 1) \right] \quad I_{00} = \frac{13}{4} + \frac{1}{2} \zeta(2) \quad (185)$$

Similarly we derive the following expression for  $S_{3p}$  of Eq.(89):

$$S_{3p} = S_{3p}^{\text{sp}} + S_{3p}^{\text{fin}}, \quad S_{3p}^{\text{fin}} = \frac{1}{\Lambda} \left[ \frac{J_2}{\Lambda} + J_1 \right] + J_0, \quad \Lambda = X^2 \lambda(1, \mu_3^2, \mu_x^2), \quad (186)$$

where the single-pole part is given in Eq.(142). For the finite part we split again the various contributions according to

$$\begin{aligned}
J_2 &= \int_0^1 dx \int_0^1 dy J_{22} + \int_0^1 dx J_{21} \\
J_1 &= \int_0^1 dx \int_0^1 dy J_{12} + \int_0^1 dx J_{11} \\
J_0 &= \int_0^1 dx J_{01} + J_{00}
\end{aligned} \quad (187)$$

The result for the  $J_i$  functions is as follows:

$$\begin{aligned}
J_{22} &= \xi(x, y) \left[ AXB(224y - 32) + 48A^2X + 66A^2B \right. \\
&\quad \left. - 64A^3y - 200XB^2 - 128X^2yB \right] L_y \ln_+ \xi(x, y) \\
&+ \xi^2(x, y) \left[ AX(42 - 192y) - 64A^2 + 340XB + 96X^2y \right] L_y \ln_+ \xi(x, y) \\
&- 140\xi^3(x, y)X L_y \ln_+ \xi(x, y) \\
&+ \left[ AX(-524yB + 32B) - 80A^2Xy - 148A^2B + 139A^3y \right. \\
&\quad \left. + 528XB^2 + 256X^2yB \right] L_x \xi(x, y) \\
&+ \xi^2(x, y) \left[ AX(-56 + 484y) + 139A^2 - 924XB - 224X^2y \right] L_x + 396\xi^3(x, y)X L_x \\
&+ \xi(x, y) \left[ AX(224yB - 32B) + 48A^2Xy + 66A^2B - 64A^3y \right. \\
&\quad \left. - 200XB^2 - 128X^2yB \right] \ln \xi(x, y) L_x \\
&+ \xi^2(x, y) \left[ AX(42 - 192y) - 64A^2 + 340XB + 96X^2y \right] \ln \xi(x, y) L_x \\
&- 140\xi^3(x, y)X \ln \xi(x, y) L_x \\
&+ \xi(x, y) \left[ AX(524yB - 32B) + 80A^2Xy + 148A^2B \right. \\
&\quad \left. - 139A^3y - 528XB^2 - 256X^2yB \right] \ln \xi(x, y)
\end{aligned}$$



$$\begin{aligned}
& +\xi^2(x, y) \left[ AX(56 - 484y) - 139A^2 + 924XB + 224X^2y \right] \ln \xi(x, y) \\
& -396\xi^3(x, y)X \ln \xi(x, y) \\
& +\xi(x, y) \left[ AX(-224yB + 32B) - 48A^2Xy - 66A^2B \right. \\
& \left. +64A^3y + 200XB^2 + 128X^2yB \right] \ln^2 \xi(x, y) \\
& +\xi^2(x, y) \left[ AX(-42 + 192y) + 64A^2 - 340XB - 96X^2y \right] \ln^2 \xi(x, y) \\
& +140\xi^3(x, y)X \ln^2 \xi(x, y) \\
& +\xi(x, y) \left[ -4AXB + 4AX^2 - A^2X + A^2B + 4X^2B - 4X^3 \right] \left( \frac{\ln \xi(x, y)}{y-1} \right)_+ \\
& +\xi(x, y) \left[ AX(24yB - 4B) + 4AX^2 - A^2X(1+y) + 8A^2B \right. \\
& \left. -6A^3y - 32XB^2 + 8X^2B(1+y) - 4X^3(1+y) \right] \ln_+ \xi(x, y) \\
& +\xi^2(x, y) \left[ -22AXy - 6A^2 + 52XB - 4X^2(1+y) \right] \ln_+ \xi(x, y) \\
& -20\xi^3(x, y)X \ln_+ \xi(x, y)
\end{aligned}$$

$$\begin{aligned}
J_{21} = & -\frac{59}{9}AX^2B + \frac{182}{75}AX^3 + \frac{31}{9}A^2XB - \frac{282}{300}A^2X^2 + \frac{283}{75}X^3B - \frac{1234}{735}X^4 \\
& + \left[ -20B^2AX - \frac{56}{3}BA^2X^2 + \frac{592}{15}AX^3 + \frac{58}{3}BA^2X \right. \\
& \left. - \frac{124}{5}A^2X^2 + 9B^2A^2 + 5A_x^3X - 5BA_x^3 + 20B^2X^2 - \frac{4}{5}BX^3 - \frac{412}{21}X^4 \right] L_x \\
& -4 \ln \xi(x, 0)A^2B^2 - \ln \xi(x, 0)L_xA^2B^2 \\
& + \left[ 20AXB^2 + 20AX^2B - 40AX^3 - 20A^2XB \right. \\
& \left. + 25A^2X^2 - 5A^2B^2 - 5A^3X + 5A^3B - 20X^2B^2 + 20X^4 \right] \ln \xi(x, 1) \\
& + \left[ 4AXB^2 + 4AX^2B - 8AX^3 - 4A^2XB \right. \\
& \left. + 5A^2X^2 - A^2B^2 - A^3X + A^3B - 4X^2B^2 + 4X^4 \right] \ln \xi(x, 1)L_x \\
& +\xi(x, 0)A^2B^2 \ln^2 + \left[ -4AXB^2 - 4AX^2B + 8AX^3 + 4A^2XB \right. \\
& \left. - 5A^2X^2 + A^2B^2 + A^3X - A^3B + 4X^2B^2 - 4X^4 \right] \ln^2 \xi(x, 1)
\end{aligned}$$

$$\begin{aligned}
J_{12} = & \xi(x, y) \left[ A(2 + 24y) - 16Xy - 30B \right] L_y \ln_+ \xi(x, y) + 30\xi^2(x, y) L_y \ln_+ \xi(x, y) \\
& +\xi(x, y) \left[ A(-7 - 64y) + 40Xy + 86B \right] L_x - 86\xi^2(x, y) L_x \\
& +\xi(x, y) \left[ A(2 + 24y) - 16Xy - 30B \right] \ln \xi(x, y)L_x + 30 \ln \xi(x, y)L_x\xi^2(x, y) \\
& +\xi(x, y) \left[ A(7 + 64y) - 40Xy - 86B \right] \ln \xi(x, y) + 86\xi^2(x, y) \ln \xi(x, y)
\end{aligned}$$

$$\begin{aligned}
& +\xi(x, y) \left[ A(-2 - 24y) + 16Xy + 30B \right] \ln^2 \xi(x, y) - 30\xi^2(x, y) \ln^2 \xi(x, y) \\
& +\xi(x, y) \left[ -A + 2X \right] \left( \frac{\ln \xi(x, y)}{y-1} \right)_+ \\
& +\xi(x, y) \left[ A(-1 + 3y) + 2X(1 + y) - 6B \right] \ln_+ \xi(x, y) + 6\xi^2(x, y) \ln_+ \xi(x, y)
\end{aligned}$$

$$\begin{aligned}
J_{11} = & -\frac{11}{36}AX - \frac{1}{6}A^2 + \frac{7}{9}XB + \frac{103}{300}X^2 \\
& + \left[ -\frac{143}{12}AX - \frac{7}{2}AB + 4A^2 + \frac{20}{3}XB + \frac{41}{15}X^2 \right] L_x \\
& + \left[ \frac{49}{4}AX + \frac{7}{2}AB - 4A^2 - \frac{22}{3}XB - \frac{42}{5}X^2 \right] \ln \xi(x, 1) \\
& + L_x \left[ 3AX + AB - A^2 - 2XB - 2X^2 \right] \ln \xi(x, 1) \\
& + \left[ -3AX - AB + A^2 + 2XB + 2X^2 \right] \ln^2 \xi(x, 1)
\end{aligned}$$

$$J_{01} = \frac{1}{3} \left[ \ln \xi(x, 1) - L_x \right] \quad J_{00} = -\frac{7}{72} \quad (188)$$

## 8 Appendix D

In this Appendix we derive results for the sunset diagram  $S_3$  at  $p^2 = 0$ . In this case we can use the notation of ref. [64], i.e.

$$\begin{aligned}
& (M_{11}, \dots, M_{1n} \mid M_{21}, \dots, M_{2m} \mid M_{31}, \dots, M_{3l}) = \\
& \int d^n p d^n q \prod_{i=1}^n \prod_{j=1}^m \prod_{k=1}^l \frac{1}{(p^2 + M_{1i}^2) (q^2 + M_{3j}^2) ((p-q)^2 + M_{2l}^2)}. \quad (189)
\end{aligned}$$

In these notations we have

$$S_3(0; m_1, m_2, m_3) = (m_1 \mid m_2 \mid m_3). \quad (190)$$

Furthermore one easily derive

$$(m_1 \mid m_2 \mid m_3) = - (m_1 \mid m_2 \mid m_3)_{(-2)} \epsilon^{-2} + (m_1 \mid m_2 \mid m_3)_{(-1)} \epsilon^{-1} + (m_1 \mid m_2 \mid m_3)_0, \quad (191)$$

with singular parts given by

$$\begin{aligned}
(m_1 \mid m_2 \mid m_3)_{(-2)} & = -2 \sum_{i=1}^3 m_i^2 \\
(m_1 \mid m_2 \mid m_3)_{(-1)} & = (m_1 \mid m_2 \mid m_3)_{(-2)} - \sum_{i=1}^3 m_i^2 \left[ 1 - 2\gamma - 2 \ln(\pi m_i^2) \right], \quad (192)
\end{aligned}$$

and a finite part that becomes

$$\begin{aligned} (m_1 | m_2 | m_3)_0 &= - (m_1 | m_2 | m_3)_{(-2)} + (m_1 | m_2 | m_3)_{(-1)} \\ &- \sum_{i=1}^3 m_i^2 \left[ -\frac{1}{2} - \frac{\pi^2}{12} - (\gamma + \ln \pi m_i^2) (\gamma + \ln \pi m_i^2 - 1) - F_i \right]. \end{aligned} \quad (193)$$

Furthermore, the finite part is given in terms of the function

$$\begin{aligned} F_i &= \int_0^1 dx \left[ \text{Li}_2(1 - \mu_i^2) - \frac{\mu_i^2}{1 - \mu_i^2} \ln \mu_i^2 \right], \\ \mu_i^2 &= \frac{a_i x + b_i(1 - x)}{x(1 - x)}, \quad a_i = \frac{m_j^2}{m_i^2}, \quad b_i = \frac{m_k^2}{m_i^2}, \end{aligned} \quad (194)$$

and

$$\begin{aligned} j = 3, k = 2 & \quad \text{for} \quad i = 1, \\ j = 1, k = 3 & \quad \text{for} \quad i = 2, \\ j = 1, k = 2 & \quad \text{for} \quad i = 3. \end{aligned} \quad (195)$$

Since  $p^2 = 0$  we can apply directly the original proposal of F. V. Tkachov [50]. First we combine the  $q_1$ -dependent propagators with a Feynman parameter  $x$  and obtain

$$\begin{aligned} \int d^n q_1 \frac{1}{(q_1^2 + m_1^2) \left( (q_1 - q_2)^2 + m_2^2 \right)} &= \\ i \pi^{2-\epsilon/2} \Gamma\left(\frac{\epsilon}{2}\right) \int_0^1 dx \left[ x(1-x) q_2^2 + (1-x) m_1^2 + x m_2^2 \right]^{-\epsilon/2}. \end{aligned} \quad (196)$$

We can *raise* one power in the integrand and obtain

$$\begin{aligned} V^{-\epsilon/2} &= 4 \frac{q^2}{(q^2 + m_2^2 - m_1^2)^2 + 4q^2 m_1^2} \\ &\times \left\{ 1 - \frac{1}{2-\epsilon} \left[ x - \frac{1}{2} \frac{q^2 - m_+ m_-}{q^2} \frac{d}{dx} \right] \right\} V^{1-\epsilon/2}, \end{aligned} \quad (197)$$

where  $m_{\pm} = m_1 \pm m_2$  and

$$V = x(1-x) q^2 + (1-x) m_1^2 + x m_2^2 = x(1-x) (q^2 + m_x^2). \quad (198)$$

Next we observe that

$$(q^2 + m_2^2 - m_1^2)^2 + 4q^2 m_1^2 = (q^2 + m_+^2) (q^2 + m_-^2), \quad (199)$$

and perform the remaining  $q$ -integration which requires the introduction of two additional Feynman parameters,  $y$  and  $z$ . This procedure will introduce two monomials in  $y, z$ ,

$$U_{\pm}(y, z) = (m_{\pm}^2 - m_x^2) y + (m_3^2 - m_{\pm}^2) z + m_x^2, \quad (200)$$

which appear with power  $-1 - \epsilon$ , so that we may use the following identity:

$$U_{\pm}^{-1-\epsilon} = \frac{1}{m_x^2} \left[ 1 + \frac{y}{\epsilon} \partial_y + \frac{z}{\epsilon} \partial_z \right] U^{-\epsilon}. \quad (201)$$

After that we proceed as usual, namely we integrate by parts and expand in Laurent series around  $\epsilon = 0$ . The final result is

$$\begin{aligned} S_3^{\text{fin}}(0; m_1, m_2, m_3) &= \frac{1}{m_+^2 - m_-^2} \left[ \int_0^1 dx \int_0^1 dy \int_0^y dz K_3 \right. \\ &\quad \left. + \int_0^1 dx \int_0^1 dy K_2 + \int_0^1 dx K_1 \right] + K_0. \end{aligned} \quad (202)$$

We now introduce auxiliary variables

$$\begin{aligned} W_{\pm}(x, y, z) &= x(1-x) [zm_3^2 + (y-z)m_{\pm}^2] + \frac{1}{4}(1-y) [(m_+ + m_-)^2 - 4m_+m_-x], \\ \chi_{\pm} &= xm_3^2 + (1-x)m_{\pm}^2, \quad A = (m_+ + m_-)^2 - 4m_+m_-x, \quad X = x(1-x), \\ L_y &= \ln(1-y), \quad L_x = \ln X, \end{aligned} \quad (203)$$

and derive

$$K_{2,3} = m_+^2 K_{2,3+} - m_-^2 K_{2,3-},$$

$$\begin{aligned} K_{3\pm} &= \ln W_{\pm}(x, y, z) \left\{ 3(L_x + L_y) [A - 12W_{\pm}(x, y, z)] - \frac{1}{2}A - 54W_{\pm}(x, y, z) \right. \\ &\quad \left. - 3 \ln W_{\pm}(x, y, z) [A - 12W_{\pm}(x, y, z)] \right\} - \frac{3}{2}A \left( \frac{\ln W_{\pm}(x, y, z)}{y-1} \right)_+ \end{aligned}$$

$$K_{2\pm} = \frac{1}{2}A \ln W_{\pm}(x, 1, y) \left\{ 3L_y + 1 + 3[L_x - \ln W_{\pm}(x, 1, y)] \right\}$$

$$\begin{aligned} K_1 &= -m_-^2(m_+m_- + \frac{3}{4}m_+^2 + \frac{1}{4}m_-^2) \ln \frac{\chi_-}{\chi_+} \ln m_1^2 \\ &\quad + m_-^2(m_+m_- - \frac{3}{4}m_+^2 - \frac{1}{4}m_-^2) \ln \frac{\chi_-}{\chi_+} \ln m_2^2 \\ &\quad - \frac{1}{4}m_+m_- \ln \chi_- [(m_+^2 - m_-^2) \ln m_1^2 - \ln m_2^2] \end{aligned}$$

$$\begin{aligned}
& +\frac{1}{4}\left[3m_+m_- + (m_+^2 + m_-^2)\right](m_+^2 - m_-^2) \ln \chi_+ \ln \frac{m_1^2}{m_2^2} \\
& -\frac{1}{2}(m_+^4 - m_-^4) \ln \chi_+ \left(1 - \frac{1}{2} \ln \chi_+\right) - \frac{1}{4}m_-^2(3m_+^2 + m_-^2) \\
& \times (\ln^2 \chi_- - \ln^2 \chi_+ - 2 \ln \frac{\chi_-}{\chi_+})
\end{aligned}$$

$$\begin{aligned}
K_0 = & +\frac{1}{2}\left[m_3^2 + \frac{1}{2}(m_+^2 + m_-^2)\right] \zeta(2) - \frac{1}{2}\left[m_+m_- + \frac{1}{2}(m_+^2 + m_-^2)\right] \ln m_1^2 \\
& +\frac{1}{2}\left[m_+m_- - \frac{1}{2}(m_+^2 + m_-^2)\right] \ln m_2^2 + \frac{1}{4}\left[m_+m_- + \frac{1}{4}(m_+^2 + m_-^2)\right] \ln^2 m_1^2 \\
& -\frac{1}{4}\left[m_+m_- - \frac{1}{2}(m_+^2 + m_-^2)\right] \ln^2 m_2^2 + \frac{13}{4}m_3^2 - \frac{17}{4}(m_+^2 + m_-^2)
\end{aligned} \tag{204}$$

The above results have been coded in a FORTRAN program and compared with those obtained with the analytical result of [64]. The comparison is shown in Tab. 8 where we use  $\epsilon = 1$  and also the  $\mu = 1$  GeV, where  $\mu$  is the unit of mass.

$m_1$ [GeV]	$m_2$ [GeV]	$m_3$ [GeV]	BT-numerical	ref. [64]
3	2	4	147.63632	147.63634
6	2	4	491.36054	491.36060
9	2	4	1437.2692	1437.2693
90	2	4	585240.60	585240.63

Table 8: The sunset topology  $S_3$  for  $p^2 = 0$ . First entry is the numerical BT-approach, second entry is the analytical result of Eqs.(193)–(194) (see ref. [64]). The UV-pole is  $\epsilon = 1$  and the unit of mass is  $\mu = 1$  GeV.

## References

- [1] A. Pais, *Oxford, Uk: Clarendon ( 1986) 666 P. New York, Usa: Oxford Univ. Pr. ( 1986) 666p.*
- [2] P. Mastrolia and E. Remiddi, Nucl. Phys. Proc. Suppl. **89** (2000) 76.
- [3] K. G. Chetyrkin and A. Retey, Nucl. Phys. B **583** (2000) 3 [hep-ph/9910332].
- [4] K. G. Chetyrkin and A. Retey, hep-ph/0007088.
- [5] G. 't Hooft and M. Veltman, Nucl. Phys. B **153** (1979) 365.
- [6] Z. Bern, L. Dixon and D. A. Kosower, Nucl. Phys. B **412** (1994) 751 [hep-ph/9306240].
- [7] Z. Bern, L. Dixon, D. C. Dunbar and D. A. Kosower, Nucl. Phys. B **425** (1994) 217 [hep-ph/9403226].
- [8] Z. Bern, L. Dixon, D. C. Dunbar and D. A. Kosower, Nucl. Phys. Proc. Suppl. **39BC** (1995) 146 [hep-ph/9409214];  
Z. Bern, L. Dixon and D. A. Kosower, Ann. Rev. Nucl. Part. Sci. **46** (1996) 109 [hep-ph/9602280];  
Z. Bern, L. Dixon, D. C. Dunbar and D. A. Kosower, hep-ph/9706447.
- [9] G. Passarino and M. Veltman, Nucl. Phys. B **160** (1979) 151.
- [10] J. Fleischer, F. Jegerlehner and O. V. Tarasov, Nucl. Phys. B **566** (2000) 423 [hep-ph/9907327].
- [11] O. V. Tarasov, Acta Phys. Polon. B **29** (1998) 2655 [hep-ph/9812250].
- [12] M. J. Veltman and D. N. Williams, hep-ph/9306228.
- [13] A. A. Vladimirov and D. V. Shirkov, Sov. Phys. Usp. **22** (1979) 860 [Usp. Fiz. Nauk **129** (1979) 407].
- [14] S. G. Gorishnii, S. A. Larin, L. R. Surguladze and F. V. Tkachov, Comput. Phys. Commun. **55** (1989) 381.
- [15] F. V. Tkachov, New methods for evaluation of multi-loop Feynman diagrams, PhD thesis, INR, Moscow, March 1984.
- [16] F. V. Tkachov, Phys. Lett. B **100** (1981) 65.
- [17] K. G. Chetyrkin and F. V. Tkachov, Nucl. Phys. B **192** (1981) 159.
- [18] F. V. Tkachov, Theor. Math. Phys. **56** (1983) 866 [Teor. Mat. Fiz. **56** (1983) 350].

- [19] D. J. Broadhurst and A. G. Grozin, hep-ph/9504400.
- [20] V. V. Belokurov and N. I. Usyukina, Theor. Math. Phys. **41** (1979) 945 [Teor. Mat. Fiz. **41** (1979) 157].
- [21] D. I. Kazakov and A. V. Kotikov, Theor. Math. Phys. **73**, 1264 (1988) [Teor. Mat. Fiz. **73**, 348 (1988)].
- [22] N. I. Usyukina and A. I. Davydychev, Phys. Lett. B **298**, 363 (1993).
- [23] V. A. Smirnov, Phys. Lett. B **500** (2001) 330 [hep-ph/0011056].
- [24] A. V. Kotikov, Phys. Lett. B **254** (1991) 158.
- [25] E. Remiddi, Nuovo Cim. A **110** (1997) 1435 [hep-th/9711188];  
M. Caffo, H. Czyz, S. Laporta and E. Remiddi, Nuovo Cim. A **111** (1998) 365 [hep-th/9805118];  
M. Caffo, H. Czyz, S. Laporta and E. Remiddi, Acta Phys. Polon. B **29** (1998) 2627 [hep-th/9807119];  
T. Gehrmann and E. Remiddi, Nucl. Phys. B **580** (2000) 485 [hep-ph/9912329];  
M. Caffo, H. Czyz and E. Remiddi, Nucl. Phys. B **581** (2000) 274 [hep-ph/9912501];  
T. Gehrmann and E. Remiddi, Nucl. Phys. Proc. Suppl. **89** (2000) 251 [hep-ph/0005232];  
T. Gehrmann and E. Remiddi, hep-ph/0008287;  
T. Gehrmann and E. Remiddi, hep-ph/0101147;  
M. Caffo, H. Czyz and E. Remiddi, hep-ph/0103014.
- [26] S. Laporta, Int. J. Mod. Phys. A **15** (2000) 5087 [hep-ph/0102033].
- [27] O. V. Tarasov, Nucl. Phys. Proc. Suppl. **89** (2000) 237.
- [28] O. V. Tarasov, Nucl. Phys. B **502** (1997) 455 [hep-ph/9703319].
- [29] F. V. Tkachov, Phys. Lett. B **124** (1983) 212.
- [30] S. G. Gorishnii, S. A. Larin and F. V. Tkachov, Phys. Lett. B **124** (1983) 217.
- [31] G. B. Pivovarov and F. V. Tkachov, *In \*Tbilisi 1986, Proceedings, Quarks '86\* 227-234.* .
- [32] F. V. Tkachov, Phys. Atom. Nucl. **56** (1993) 1558 [Yad. Fiz. **56** (1993) 180].
- [33] F. V. Tkachov, Phys. Lett. B **412**, 350 (1997) [hep-ph/9703424].
- [34] J. Fleischer, V. A. Smirnov, A. Frink, J. G. Korner, D. Kreimer, K. Schilcher and J. B. Tausk, Eur. Phys. J. C **2** (1998) 747 [hep-ph/9704353];  
M. Beneke and V. A. Smirnov, Nucl. Phys. B **522** (1998) 321 [hep-ph/9711391];  
V. A. Smirnov and E. R. Rakhmetov, Theor. Math. Phys. **120** (1999) 870 [Teor. Mat. Fiz.

- 120** (1999) 64] [hep-ph/9812529];  
 A. I. Davydychev and V. A. Smirnov, Nucl. Phys. B **554** (1999) 391 [hep-ph/9903328];  
 V. A. Smirnov, Phys. Lett. B **460** (1999) 397 [hep-ph/9905323];  
 V. A. Smirnov and O. L. Veretin, Nucl. Phys. B **566** (2000) 469 [hep-ph/9907385];  
 V. A. Smirnov, Phys. Lett. B **465** (1999) 226 [hep-ph/9907471];
- [35] P. A. Baikov and V. A. Smirnov, Phys. Lett. B **477** (2000) 367 [hep-ph/0001192];  
 V. A. Smirnov, Phys. Lett. B **491** (2000) 130 [hep-ph/0007032];
- [36] V. A. Smirnov, hep-ph/0101152.
- [37] F. V. Tkachov and K. G. Chetyrkin, *In \* Zvenigorod 1979, Proceedings, Group Theoretical Methods In Physics, Vol. 2\*, 223-227.*
- [38] K. G. Chetyrkin, A. L. Kataev and F. V. Tkachov, Nucl. Phys. B **174** (1980) 345.
- [39] G. B. Pivovarov and F. V. Tkachov, Int. J. Mod. Phys. A **8** (1993) 2241 [hep-ph/9612287].
- [40] J. Fleischer, O. V. Tarasov and M. Tentyukov, Nucl. Phys. Proc. Suppl. **89** (2000) 112.
- [41] O. V. Tarasov, Nucl. Phys. B **480** (1996) 397 [hep-ph/9606238].
- [42] O. V. Tarasov, Phys. Rev. D **54** (1996) 6479 [hep-th/9606018].
- [43] J. Fleischer and O. V. Tarasov, Nucl. Phys. Proc. Suppl. **37B** (1994) 115 [hep-ph/9407235].
- [44] D. J. Broadhurst, Phys. Lett. B **164** (1985) 356;  
 D. J. Broadhurst, Z. Phys. C **47** (1990) 115;  
 D. J. Broadhurst, Z. Phys. C **54** (1992) 599;  
 D. J. Broadhurst, J. Fleischer and O. V. Tarasov, Z. Phys. C **60** (1993) 287 [hep-ph/9304303];  
 D. J. Broadhurst and D. Kreimer, Phys. Lett. B **426** (1998) 339 [hep-th/9612011].
- [45] G. Degrandi, P. Gambino and A. Vicini, Phys. Lett. B **383** (1996) 219 [hep-ph/9603374];  
 G. Degrandi, P. Gambino and A. Sirlin, Phys. Lett. B **394** (1997) 188 [hep-ph/9611363];  
 G. Degrandi and P. Gambino, Nucl. Phys. B **567** (2000) 3 [hep-ph/9905472].
- [46] A. Freitas, S. Heinemeyer, W. Hollik, W. Walter and G. Weiglein, Nucl. Phys. Proc. Suppl. **89** (2000) 82 [hep-ph/0007129];  
 A. Freitas, W. Hollik, W. Walter and G. Weiglein, Phys. Lett. B **495** (2000) 338 [hep-ph/0007091];  
 A. Freitas, S. Heinemeyer, W. Hollik, W. Walter and G. Weiglein, hep-ph/0101260;  
 S. Heinemeyer and G. Weiglein, hep-ph/0102317.



- [47] T. van Ritbergen and R. G. Stuart, Phys. Rev. Lett. **82** (1999) 488 [hep-ph/9808283].
- [48] F. A. Berends, A. I. Davydychev and N. I. Ussyukina, Phys. Lett. B **426** (1998) 95 [hep-ph/9712209];  
 S. Groote, J. G. Korner and A. A. Pivovarov, Phys. Lett. B **443** (1998) 269 [hep-ph/9805224];  
 S. Groote, J. G. Korner and A. A. Pivovarov, Nucl. Phys. B **542** (1999) 515 [hep-ph/9806402];  
 A. I. Davydychev and V. A. Smirnov, Nucl. Phys. B **554** (1999) 391 [hep-ph/9903328];  
 S. Groote, J. G. Korner and A. A. Pivovarov, Eur. Phys. J. C **11** (1999) 279 [hep-ph/9903412];  
 A. Bashir, R. Delbourgo and M. L. Roberts, hep-th/0101148;  
 M. Caffo, H. Czyz, S. Laporta and E. Remiddi, Nuovo Cim. A **111** (1998) 365 [hep-th/9805118];  
 M. Caffo, H. Czyz and E. Remiddi, Nucl. Phys. B **581** (2000) 274 [hep-ph/9912501];  
 M. Caffo, H. Czyz and E. Remiddi, hep-ph/0103014.
- [49] R. J. Eden, P. V. Landshoff, D. I. Olive, and J. C. Polkinghorne, The analytic S matrix, Cambridge Univ. Press, 1966. 287p.
- [50] F. V. Tkachov, Nucl. Instrum. Meth. A **389** (1997) 309 [hep-ph/9609429];  
 L. N. Bertstein, Functional Analysis and its Applications, **6**(1972)66.
- [51] D. Y. Bardin, L. V. Kalinovskaya and F. V. Tkachov, hep-ph/0012209.
- [52] G. Passarino, hep-ph/0101299.
- [53] D. Bardin and G. Passarino, *Oxford, UK: Clarendon (1999) 685 p.*
- [54] F. V. Tkachov, Int. J. Mod. Phys. A **8** (1993) 2047 [hep-ph/9612284];  
 F. V. Tkachov, Sov. J. Part. Nucl. **25** (1994) 649 [hep-ph/9701272].
- [55] G. Devaraj and R. G. Stuart, Nucl. Phys. B **519** (1998) 483 [hep-ph/9704308].
- [56] P. Cvitanovic and T. Kinoshita, Phys. Rev. D **10** (1974) 3978.
- [57] G. Passarino and S. Uccirati, Numerical Evaluation of Two-Loop Self-Energies, work in preparation.
- [58] G. 't Hooft and M. Veltman, Nucl. Phys. B **44** (1972) 189.
- [59] A. Ghinculov and Y. Yao, Phys. Rev. D **63** (2001) 054510 [hep-ph/0006314];  
 A. Ghinculov and Y. Yao, Mod. Phys. Lett. A **15** (2000) 1967 [hep-ph/0004201];  
 A. Ghinculov and Y. Yao, Mod. Phys. Lett. A **15** (2000) 925 [hep-ph/0002211];  
 A. Ghinculov and Y. Yao, Nucl. Phys. B **516** (1998) 385 [hep-ph/9702266].
- [60] J. A. Vermaseren, math-ph/0010025.

- [61] F. A. Berends, A. I. Davydychev and V. A. Smirnov, Nucl. Phys. Proc. Suppl. **51C** (1996) 301 [hep-ph/9606244];  
F. A. Berends, A. I. Davydychev and V. A. Smirnov, Nucl. Phys. B **478** (1996) 59 [hep-ph/9602396];  
S. Bauberger, F. A. Berends, M. Bohm and M. Buza, Nucl. Phys. B **434** (1995) 383 [hep-ph/9409388];  
S. Bauberger, M. Bohm, G. Weiglein, F. A. Berends and M. Buza, Nucl. Phys. Proc. Suppl. **37B** (1994) 95 [hep-ph/9406404];  
F. A. Berends and J. B. Tausk, Nucl. Phys. B **421** (1994) 456.
- [62] M. Caffo, H. Czyz, S. Laporta and E. Remiddi, Nuovo Cim. A **111** (1998) 365 [hep-th/9805118].
- [63] NAG Fortran Library, Mark 19, The Numerical Algorithms Group Ltd, Oxford UK. 1999.
- [64] J. van der Bij and M. Veltman, Nucl. Phys. B **231** (1984) 205.

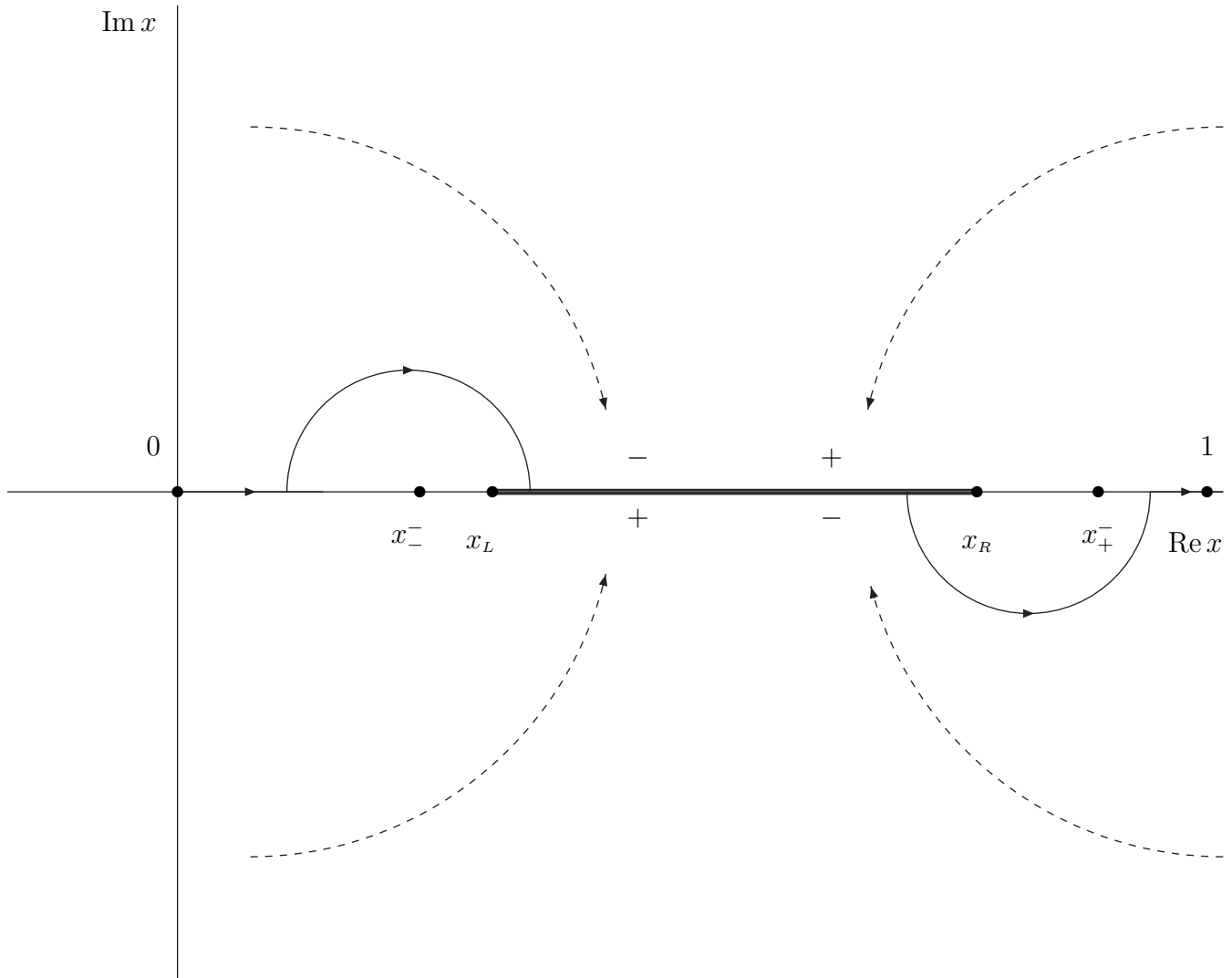


Figure 9: The complex  $x$ -plane with the cut of  $\ln \chi$  (Eq.(34)) internal to the interval  $[x_-, x_+^-]$  (Eq.(119)). Dashed lines indicate the sign of the imaginary part of the logarithm when approaching the real axis on the cut. An example of the deformation of the integration path is shown.

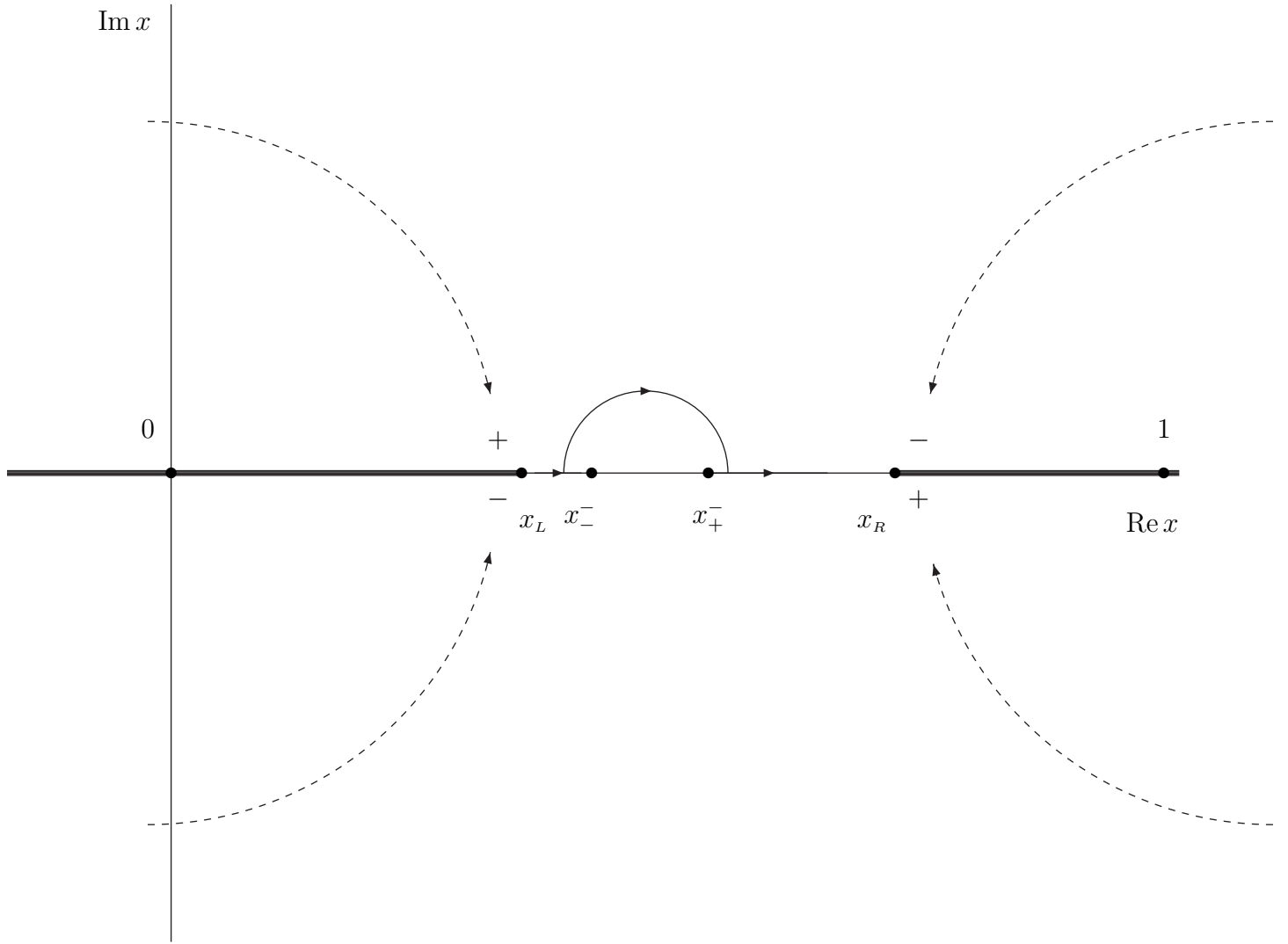


Figure 10: The complex  $x$ -plane with the cut of  $\ln \chi$  (Eq.(34)) external to the interval  $[x_-^-, x_+^-]$  (Eq.(119)). Dashed lines indicate the sign of the imaginary part of the logarithm when approaching the real axis on the cut. An example of the deformation of the integration path is shown.

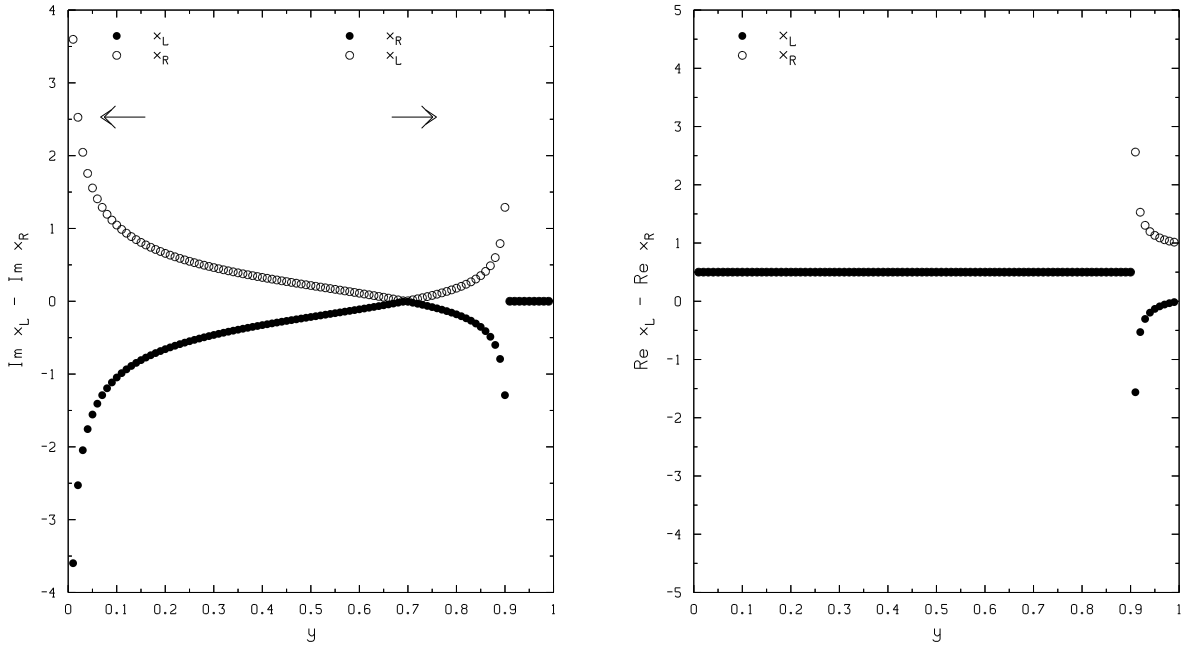


Figure 11: The behavior of  $x_L$  and  $x_R$ , the roots of the quadratic of Eq.(144)) as a function of  $y$  for the sunset diagram at the normal threshold  $s = (m_1 + m_2 + m_3)^2$ . The figure shows that the integration contour is pinched by the two branch points  $x_{L,R}$  which are the roots of Eq.(144).

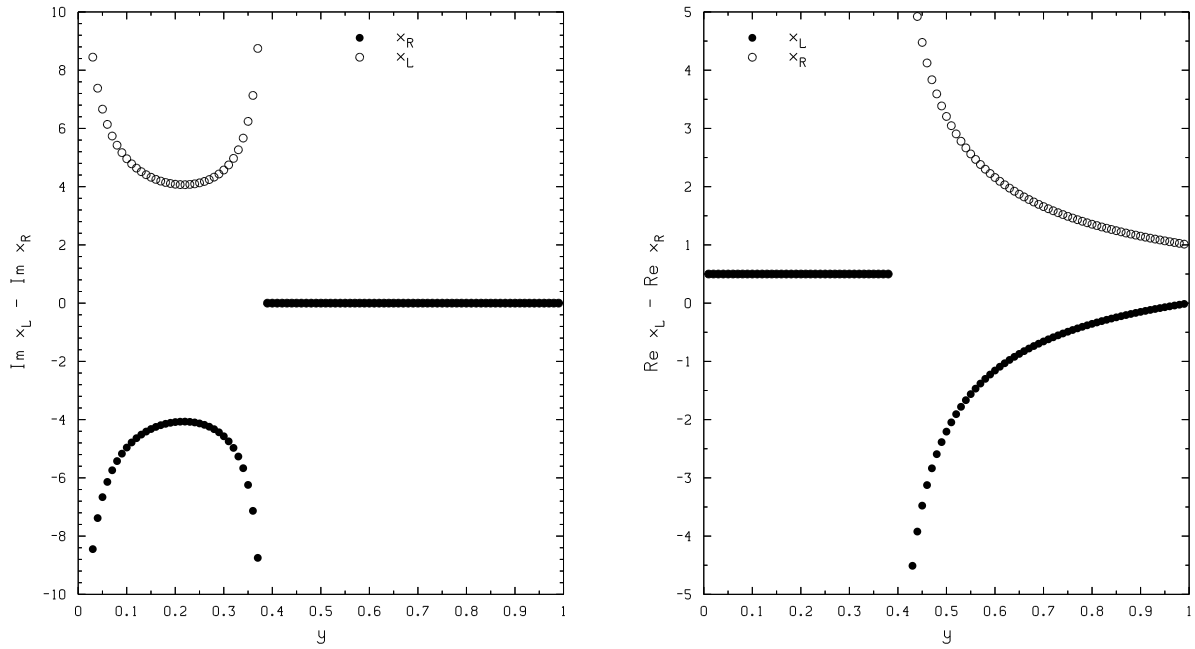


Figure 12: The behavior of  $x_L$  and  $x_R$ , the roots of the quadratic of Eq.(144) as a function of  $y$  for the sunset diagram at the pseudo threshold  $s = (m_1 + m_2 - m_3)^2$ .